

INFORMATION TO USERS

This manuscript has been reproduced from the microfilm master. UMI films the text directly from the original or copy submitted. Thus, some thesis and dissertation copies are in typewriter face, while others may be from any type of computer printer.

The quality of this reproduction is dependent upon the quality of the copy submitted. Broken or indistinct print, colored or poor quality illustrations and photographs, print bleedthrough, substandard margins, and improper alignment can adversely affect reproduction.

In the unlikely event that the author did not send UMI a complete manuscript and there are missing pages, these will be noted. Also, if unauthorized copyright material had to be removed, a note will indicate the deletion.

Oversize materials (e.g., maps, drawings, charts) are reproduced by sectioning the original, beginning at the upper left-hand corner and continuing from left to right in equal sections with small overlaps. Each original is also photographed in one exposure and is included in reduced form at the back of the book.

Photographs included in the original manuscript have been reproduced xerographically in this copy. Higher quality 6" x 9" black and white photographic prints are available for any photographs or illustrations appearing in this copy for an additional charge. Contact UMI directly to order.

UMI

A Bell & Howell Information Company
300 North Zeeb Road, Ann Arbor MI 48106-1346 USA
313/761-4700 800/521-0600



University of Alberta

**Mapping and Detecting Change in the Aeolian Sand Deposits
of Southern Alberta Using Wet Year-Dry Year Landsat
Thematic Mapper Imagery**

by

Melodie Lynne Sept



A thesis submitted to the Faculty of Graduate Studies and Research in partial
fulfillment of the requirements for the degree of Master of Science

Department of Earth and Atmospheric Sciences

Edmonton, Alberta

Fall, 1997



National Library
of Canada

Acquisitions and
Bibliographic Services

395 Wellington Street
Ottawa ON K1A 0N4
Canada

Bibliothèque nationale
du Canada

Acquisitions et
services bibliographiques

395, rue Wellington
Ottawa ON K1A 0N4
Canada

Your file *Votre référence*

Our file *Notre référence*

The author has granted a non-exclusive licence allowing the National Library of Canada to reproduce, loan, distribute or sell copies of this thesis in microform, paper or electronic formats.

The author retains ownership of the copyright in this thesis. Neither the thesis nor substantial extracts from it may be printed or otherwise reproduced without the author's permission.

L'auteur a accordé une licence non exclusive permettant à la Bibliothèque nationale du Canada de reproduire, prêter, distribuer ou vendre des copies de cette thèse sous la forme de microfiche/film, de reproduction sur papier ou sur format électronique.

L'auteur conserve la propriété du droit d'auteur qui protège cette thèse. Ni la thèse ni des extraits substantiels de celle-ci ne doivent être imprimés ou autrement reproduits sans son autorisation.

0-612-22671-9

University of Alberta

Library Release Form

Name of Author: Melodie Lynne Sept

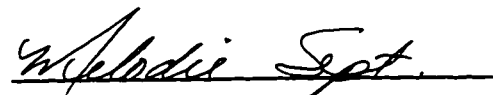
Title of Thesis: Mapping and Detecting Change in the Aeolian Deposits of Southern
Alberta Using Wet Year-Dry Year Landsat Thematic Mapper Imagery

Degree: Master of Science

Year this Degree Granted: 1997

Permission is hereby granted to the University of Alberta Library to reproduce single copies of this thesis and to lend or sell such copies for private, scholarly, or scientific research purposes only.

The author reserves all other publication and other rights in association with the copyright in the thesis, and except as hereinbefore provided, neither the thesis nor any substantial portion thereof may be printed or otherwise reproduced in any material form whatever without the author's prior written permission.



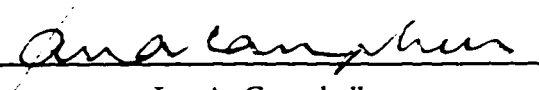
221, 11405 - 27 Avenue
Edmonton Alberta
T6J 3N6

Sept 24, 1997.

University of Alberta

Faculty of Graduate Studies and Research


The undersigned certify that they have read, and recommend to the Faculty of Graduate Studies and Research for acceptance, a thesis entitled **Mapping and Detecting Change in the Aeolian Sand Deposits of Southern Alberta Using Wet Year-Dry Year Landsat Thematic Mapper Imagery** submitted by Melodie Lynne Sept in partial fulfillment of the requirements for the degree of Master of Science.



Ian A. Campbell



Benoit Rivard



M. Anne Naeth

Approval Date:

June 6 1987

ABSTRACT

Landsat Thematic Mapper imagery acquired for a wet and dry year were used to map and detect change in aeolian sand deposits of southern Alberta. Post-classification comparison between the two years showed that both image sets discriminated between the various deposits, but with differences in their extent. Deposits unique to each year were also visible. Principle component analysis of the merged data provided similar results; features common to both years appeared in the first component and areas of change appeared in the higher order components. Areas of change between the images were associated with differences in moisture content between the aeolian deposits. The results suggest that the relationship between the surficial deposits, moisture conditions and vegetation is complex. Multi-temporal imagery, supplemented with auxiliary data, is needed to better understand which field parameters control the spectral response seen by the satellite and for quantifying changes occurring in these aeolian deposits.

ACKNOWLEDGEMENTS

The past two years spent researching this thesis have been very rewarding for me, and I would like to express my gratitude to those who helped make it so. First, my thanks go to Ian Campbell for his patience and support throughout my research, and for providing me with opportunities I otherwise would not have had. The field trip to the American southwest and working in Italy have been high points of my experience here. Together with Laurel Murphy and Celina Campbell, he made these two years a lot of fun. Thank you to Benoit Rivard for introducing me to different aspects of remote sensing, and Anne Naeth, who sparked my interest as to the intricacies of grassland vegetation. I would also like to thank John Hodgson, whose words of support have always been an encouragement to me, and the Department of Earth and Atmospheric Sciences for the financial assistance which made this thesis possible.

Finally, I would like to thank my friend Randi Mewhort who has always given me a shoulder to cry on or a pat on the back, which ever was needed, and my husband Dave, who kept me sane while I drove him crazy. Thank you for always just being there.

TABLE OF CONTENTS

CHAPTER 1. INTRODUCTION	1
Aeolian Deposits as Indicators of Climate Change	1
Aeolian Deposits in Alberta	2
Objectives	4
CHAPTER 2. NATURE OF RESEARCH AND LITERATURE REVIEW	6
Introduction	6
Reflectance Patterns of Vegetation and Soil	6
Mapping Aeolian Deposits using Satellite Imagery	11
Detecting Change in Aeolian Environments using Satellite Imagery	12
Conclusion	14
CHAPTER 3. SITE DESCRIPTION	16
Location and Description of Study Area	16
Vegetation and Soils	19
Present Climate	25
Conclusion	26
CHAPTER 4. IMAGE SELECTION AND PREPROCESSING	27
Introduction	27
Image Selection	28
Image Correction and Rectification	29
Creating the Digital Elevation Model	34
Conclusion	36
CHAPTER 5. MULTI-TEMPORAL IMAGE PROCESSING	38
Introduction	38
Cluster Analysis	39

LIST OF TABLES

	Page
Table 3-1. Spectral Interpretation of Features in the Rolling Hills Colour Composite shown in Figure 3-3.	20
Table 4-1. Thematic Mapper Spectral Bands After Lillesand and Kiefer (1994).	29
Table 4-2. Landsat Thematic Mapper Imagery Specifications for 1986 and 1988.	30
Table 4-3. Digital Numbers used in Atmospheric Correction	32
Table 5-1. Area Comparison of Each Spectral Land Cover Class	45
Table 5-2. Confusion Matrix for 1986 Cluster Analysis	46
Table 5-3. Confusion Matrix for 1988 Cluster Analysis	47
Table 6-1. Eigen Structure for Multi-temporal Principle Component Analysis.	61
Table 6-2. Eigen Structure for Selective Principle Component Analysis.	63
Table I-1. Coordinates of the Ground Control Points Used to Rectify the 1986 Landsat TM Scene.	80
Table I-2. Coordinates of the Ground Control Points Used to Rectify the 1988 Landsat TM Scene.	81
Table I-3. Coefficients Used to Rectify the 1986 and 1988 Landsat TM Scenes.	82
Table II-1. Landsat TM Post-calibration Spectral Radiances and Solar Irradiances..	84

LIST OF FIGURES

		Page
Figure 1-1.	Distribution of sand deposits in southern Alberta Based on Mulira (1986).	3
Figure 2-1.	Typical reflectance and transmittance spectra of an individual plant leaf. After Walter-Shea and Norman (1991).	8
Figure 2-2.	Reflectance and transmittance spectra for individual leaves of the prairie grass, Big Bluestem. After Walter- Shea and Norman (1991).	8
Figure 2-3.	Changes in spectral response of a sycamore leaf in response to varying moisture content. After Elachi (1987).	10
Figure 2-4.	Generalized reflectance curves for dry and wet soils Landsat TM bands are included for comparison. After Drury (1993) and Lillesand and Kiefer (1994).	10
Figure 3-1.	Location of the Rolling Hills dune field.	17
Figure 3-2.	Surficial geology of the Rolling Hills region Based on Shetsen (1987).	18
Figure 3-3.	Colour infrared composite of the Rolling Hills area, created by assigning band 5 to blue, band 3 to green, and band 4 to red. Area A corresponds with the main dune field, B corresponds with a minor dune area, and C corresponds with sand sheets. Landsat image acquired July 31, 1986.	20
Figure 3-4.	Oblique aerial photograph of a parabolic dune in the main dune area, with dune-track ridges clearly visible. These ridges mark the former positions of the dune base. Photo taken on June 14, 1996.	21
Figure 3-5.	Typical vegetation of the grassland plains. Species shown include Needle-and-thread and Blue grama grass with scattered patches of Pasture sage. Photo taken on July 3, 1996.	23
Figure 3-6.	Typical vegetation in the Rolling Hills dune field. Species shown include Silver sagebrush, Pasture sage, Alberta wild rose and Shrubby cinquefoil. Photo taken on July 3, 1996.	23

Figure 4-1.	Departures from mean annual precipitation for the Medicine Hat region, 1961-1990. From Proudfoot (1994).	30
Figure 4-2.	Illustration of the effects of atmospheric scattering on TM band 3 for 1986, (a) before correction, and (b) after correction.	32
Figure 5-1.	K-means or migrating means cluster analysis; (a) shows the initial 'seeding' of the mean vectors and the pixel assignment, (b) shows the result of the second iteration. The process continues until there is no significant change in the position of the mean vectors between iterations. After Richards (1986).	40
Figure 5-2.	Plot of F-ratios versus cluster number. Peaks in the data indicate the number of clusters where the between sample variance is high while within sample variance is low.	40
Figure 5-3.	Land cover map of the Rolling Hills dune field obtained through K-means cluster analysis of Landsat TM bands 3, 4, and 5 for 1986.	43
Figure 5-4.	Land cover map of the Rolling Hills dune field based on K-means cluster analysis of Landsat TM bands 3, 4, and 5 for 1988.	44
Figure 5-5.	Comparison of reflectance curves for eight spectral classes for (a) band 3, (b) band 4, and (c) band 5.	48
Figure 5-6.	Dune change classes for the Rolling Hills dune field. Blue areas correspond to those deposits which were common to both 1986 and 1988. Red areas correspond with deposits which appeared only in the 1986 imagery and purple areas correspond with deposits which appeared only in the 1988 imagery. Scale of the image is 1:200 000.	49
Figure 6-1.	The principle component transformation; (a) bivariate plot of correlated data, with axes shifted to mean of the data set, (b) axes are rotated so that PC1 is oriented along the major axis of the ellipse. PC2 is orthogonal to PC1. From Drury (1993).	54

Figure 6-2 (a).	Eigen images for PCs 1 and 2, for the 1986 and 1988 merged data set. PC1 is a measure of greenness, where features with high biomass appear dark, and areas of low biomass are bright. PC2 shows overall brightness. Scale of images is 1:200 000.	58
Figure 6-2 (b).	Eigen images for PCs 3 and 4. PC3 shows decreases in greenness due to differences between the wet and dry year. PC4 shows changes in brightness between the two years. Scale of images is 1: 200 000.	59
Figure 6-2 (c).	Eigen images for PCs 5 and 6. PC5 is related to differences in moisture between the wet and dry year. PC6 shows mostly noise. Scale of images is 1: 200 000.	60
Figure 6-3.	Principle component colour composite. PC3 was assigned to blue, PC1 was assigned to green and PC2 was assigned to red. Scale of image is 1: 200 000.	62
Figure 6-4.	PC2 from selective principle component analysis of band 5 for 1986 and 1988. Scale of image is 1: 200 000.	64
Figure 6-5.	Change classes created from an unsupervised classification of PC2 of band 5 for 1986 and 1988. Scale of image is 1: 200 000.	65
Figure III-1.	Hillshade model of the Rolling Hills area in southern Alberta. Area A corresponds to the main dune field. Model created using a digital elevation model generated from a 1 m interval contour topographic map (Porter 1995). Scale of image is 1: 200 000.	85

CHAPTER 1

INTRODUCTION

Aeolian Deposits as Indicators of Climate Change

Aeolian sand deposits in North America cover only 2% of the continents' arid regions (Thomas 1989) but they have proven to be important sources of information for improving our understanding of paleoclimatical and paleoenvironmental conditions. The stratigraphy of these deposits serve as proxy evidence of both short term and long term fluctuations in climate (Gaylord 1990; Jorgensen 1992; Stokes and Gaylord 1993; Gaylord 1994). With recent concerns about the potential effects of global warming, a better understanding of how climate has changed during the Quaternary may be useful for assessing the impact of future climate change (Madole 1994).

Most studies of aeolian sand deposits in North America show that periods of severe drought occurred during the Holocene resulting in degradation of vegetative cover and widespread mobilization of these deposits (Gaylord 1982; Gaylord 1990; Madole 1994). Dune stratigraphy in the Ferris Dune Field, Wyoming, for example, showed that average wind speeds and direction did not vary significantly during the Holocene, but variations in precipitation, and therefore plant growth, resulted in several periods of renewed dune sedimentation (Gaylord 1982; 1990). From approximately 7500 BP to the present time, there have been repeated episodes of aridity and dune activity followed by relatively more humid conditions and dune stability (Gaylord 1990; Stokes and Gaylord 1993). Similar trends have also been noted in the Hanford Site, Washington (Gaylord and Stetler 1994), along the South Platte River, Colorado (Madole 1994) and in the Great Sand Hills, Saskatchewan (Wolfe et al. 1995).

Aeolian Deposits in Alberta

Large areas of semiarid southern Alberta are covered by postglacial aeolian deposits of sand, which typically form sheets and dunes (Figure 1-1). These sands are generally derived from glaciofluvial and glaciolacustrine sediments which were deposited into proglacial lakes that formed as the Laurentide Ice Sheet retreated, sometime around 20 - 18 ka BP (Christiansen 1979; Clayton and Moran 1982; Evans and Campbell 1992). As ice retreated further to the north and the east, and as drainage channels at lower elevations opened up, about 15 ka BP (Bryan et al. 1987; Evans and Campbell 1992), the proglacial lakes drained, exposing large areas of fine-grained lacustrine materials. These were preferentially removed and reworked into various forms of aeolian deposits, typically of the parabolic dune association (David 1977; Wolfe et al. 1995).

At present, the distribution and phases of stability and reactivation of these deposits is not well understood. Such knowledge would prove useful in landscape interpretation, paleoclimate research, and climate change studies as well as assisting in making land use management decisions. Many studies have focused on dune morphology and stratigraphy or paleosol development as being the key indicators of past dune activity and stabilization (Gaylord 1990; Jorgensen 1992; David 1993; Stokes and Gaylord 1993; Gaylord and Stettler 1994; Madole 1994; Muhs and Holliday 1995; Roesler 1995; Wolfe et al. 1995). However, dunes are particularly sensitive to changes in climate which may lead to the degradation of vegetation and their possible re-mobilization. Changes that occur in the vegetation cover due to variations in soil moisture availability may provide insight to these dune's response to drought, and perhaps climatic changes. Changes in the vegetative cover between dunes and surrounding areas, or changes in cover from year to year, have been detected and monitored using remote sensing and comparing wet year to dry year imagery (Franklin 1991; Jacobberger and Hooper 1991; Forman et al. 1992; Dwivendi et al. 1993; Chavez and Mackinnon 1994). As yet, only one study has applied satellite data to Canadian dunes (Murphy 1996). This study is a continuation of that work; it seeks to identify, map, and interpret the distribution and geomorphology of

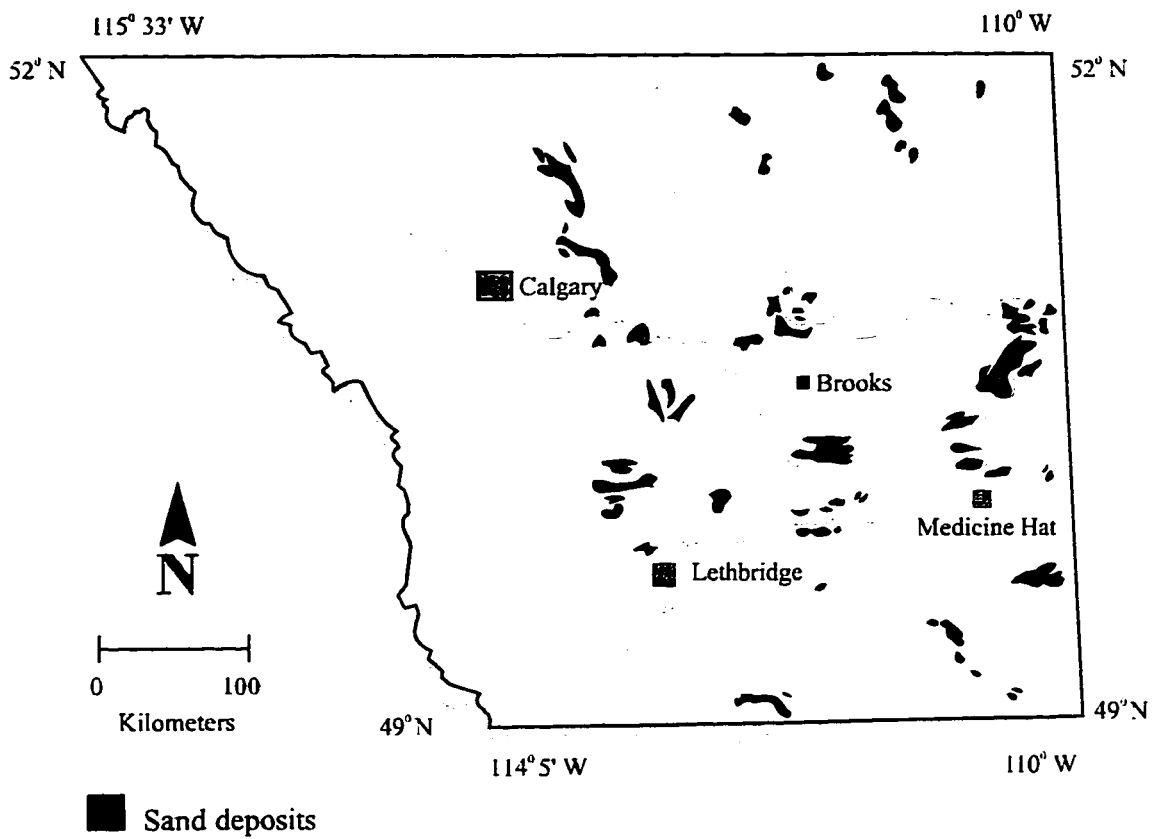


Figure 1-1. Distribution of sand deposits in southern Alberta. Based on Mulira (1986).

aeolian sand deposits in southern Alberta and examine the response of these deposits to moisture deficits.

Past efforts to inventory and map the distribution of aeolian deposits in southern Alberta revealed a great deal of variation in their location and extent. The problem related to the large extent of the area, the lack of high quality primary data and the mobile nature of these deposits. For example, David (1977) compiled an inventory of sand dune occurrences in Canada, but omitted areas that covered less than 16 km². In Alberta, some deposits exceeding this size were omitted because it was felt they lacked important land forms. Mulira (1986) mapped sand dune occurrences in Alberta, but commented that the primary data available was of poor quality and that some deposits were too mobile to be accurately mapped. Shetsen's (1987) work on Quaternary deposits in central and southern Alberta is the most comprehensive work to date, including many of the dune fields, but the location and extent of dune areas shown on her maps do not agree with previous work. Another related problem is that previous mapping and interpretations were based on conventional air photographs and field surveys. However, many of these deposits could not be clearly defined on air photos because of their low relief and mobility. Interpretation based on satellite imagery as shown by Murphy (1996), and this study, resolves some of these problems.

Objectives

The purpose of this study was twofold. First, to identify and map aeolian sand deposits in the Rolling Hills area of southern Alberta based upon the spectral reflectance of vegetation and soils. Secondly, to examine the ability to detect climate related changes, specifically changes in vegetation due to variations in precipitation levels in these deposits, using satellite imagery acquired for a wet year and a dry year. Satellite imagery provides several advantages over more traditional mapping methods. First, it allows synoptic coverage of a large area, with potentially 30 years of data and regular repeat coverage making it a relatively cost effective mapping and monitoring tool. Second, images are

multispectral using wavelengths in both the visible and infrared portion of the electromagnetic spectrum to identify features. Finally, satellite imagery is in digital form allowing several image enhancement and statistical techniques to be applied.

The specific objectives of this study were:

1. To examine the potential of using multispectral satellite imagery in delimiting aeolian and non-aeolian deposits in the Rolling Hills dune field, and the application of these techniques to other regions.
2. To examine the potential of using multi-temporal data sets in detecting and monitoring climate related changes in moisture in these deposits.

CHAPTER 2

NATURE OF RESEARCH AND LITERATURE REVIEW

Introduction

Dune deposits have received a great deal of attention in the literature due to their potential as indicators of past and present climate change (Gaylord 1990; Jorgensen 1992; Muhs and Maat 1993; Stokes and Gaylord 1993; Gaylord and Stetler 1994; Madole 1994; Wolfe et al. 1995). However, a better understanding of these deposits is also important for interpreting the landscape and assisting in decision-making relevant to land management. Satellite imagery is becoming increasingly important in this regard due to its synoptic and repeat coverage and multispectral nature. This chapter will present the basic concepts of vegetative and soil responses to electromagnetic radiation to assist in the understanding of the application of satellite imagery to mapping dune deposits. In addition, results of previous studies employing satellite imagery in dune areas will be discussed to introduce the potential of applying remotely sensed data in this research.

Reflectance Patterns of Vegetation and Soil

Dune deposits are easily identified on Landsat Thematic Mapper (TM) imagery due to their striking morphology and differences in stabilizing vegetation between the dunes and inter-dune corridors (Jacobberger and Hooper 1991). Differences in vegetation composition, density, and vigor between dunes and the inter-dune areas may be related to variations in soil moisture. Water is able to percolate to lower levels in the dune sands, and favours the growth of plants able to access this moisture, i.e. longer tap roots

(Coupland 1950, 1961). Additionally, increased moisture availability may favour denser or more vigorous vegetational cover. These differences in plant cover between sand dunes and surrounding deposits can be detected using Landsat TM data (Franklin 1991; Jacobberger and Hooper 1991; Forman et al. 1992; Dwivendi et al. 1993; Chavez and MacKinnon 1994; Murphy 1996).

The interactions of radiative energy with vegetation is extremely complex. Energy is reflected, transmitted or absorbed by leaves as a function of wavelength, leaf cellular structure, leaf moisture, pubescence, surface roughness, morphology, and physiology (Walter-Shea and Norman 1991). Related factors include the density and homogeneity of the canopy and canopy structure (Kimes 1991), soil background effects (Tueller 1987; Heute 1988) and illumination and viewing angles (Elachi 1987; Kimes 1991; Walter-Shea and Norman 1991). To simplify this discussion, it is useful to consider the interaction of electromagnetic radiation with a single leaf. The patterns seen are similar for all leaves with variations in magnitude arising for different species and leaf age (Walter-Shea and Norman 1991).

Figure 2-1 shows the typical reflectance and transmittance curves for a single leaf. There are three regions of interaction; from 0.3-0.7 μm (visible), 0.7-1.35 μm (near infrared, NIR) and 1.35-2.7 μm (mid-infrared, mid-IR). In the visible part of the spectrum little radiation is reflected or transmitted by healthy green leaves due to absorption by plant pigments, especially chlorophyll. A peak in reflectance corresponding to the green part of the spectrum (approximately 0.55 μm) explains the green colour of leaves (Elachi 1987; Walter-Shea and Norman 1991; Drury 1993; Lillesand and Kiefer 1994). Absorption, transmittance and reflectance will vary with the age of a leaf. Figure 2-2 shows these variations in grass leaves as the leaves mature and become senescent. Pigments accumulate as the leaf grows resulting in a decrease in reflectance with age. With the onset of senescence, chlorophyll begins to deteriorate and reflectance increases (Walter-Shea and Norman 1991).

In the NIR and mid-IR reflectance and transmittance are high. In the NIR reflectance and transmittance are high due to multiple scattering of light by leaf mesophyll

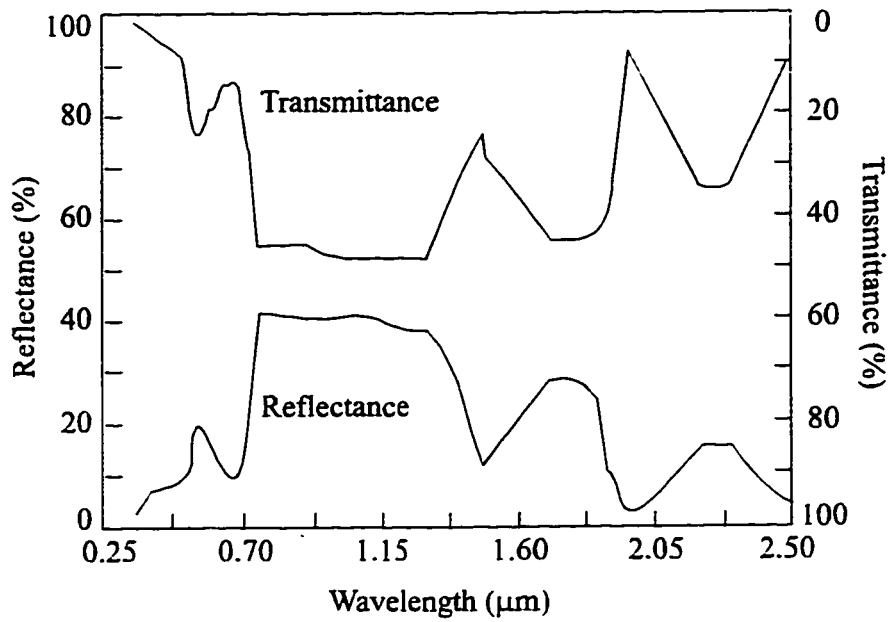


Figure 2-1. Typical reflectance and transmittance spectra of an individual plant leaf. After Walter-Shea and Norman (1991).

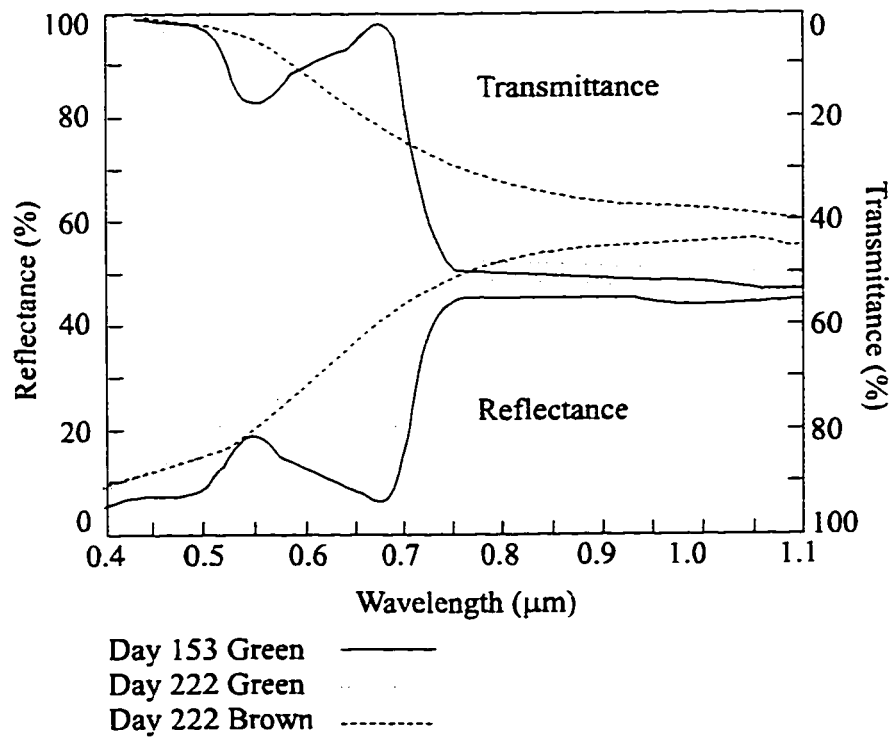


Figure 2-2. Reflectance and transmittance spectra for individual leaves of the prairie grass, Big bluestem. After Walter-Shea and Norman (1991).

cells and the low absorption coefficient (Walter-Shea and Norman 1991). Scattering occurs at sites where discontinuities in the refractive index arise, primarily between air and the cell walls (Elachi 1987; Walter-Shea and Norman 1991). As the leaf grows intercellular spaces develop and enlarge, causing increases in NIR reflectance as the leaves mature (Walter-Shea and Norman 1991). In the mid-IR reflectance and transmittance is slightly lower than that in the NIR, due to attenuation of light by water in the leaves and internal leaf structure (Elachi 1987; Walter-Shea and Norman 1991). Leaf water content has a direct impact on reflectance and transmittance due to water absorption bands in the 1.35-2.5 μm region (1.43 μm , 1.95 μm and 2.2 μm). Decreases in leaf water content results in direct increases in reflectance and transmittance in the mid-IR and indirect increases in reflectance in the other bands due to increases in internal leaf spaces due to decreases in leaf water content or cell breakdown. The magnitude of these effects varies with species (Elachi 1987; Walter-Shea and Norman 1991). Figure 2-3 demonstrates how reflectance changes with decreases in cell water content for a sycamore leaf.

Typical reflectance curves for wet and dry soil are shown in Figure 2-4. In general the reflectance of dry soils shows less variation over the spectrum (0.4-2.4 μm), reflectance tends to increase as wavelength increases. The curve for moist soil is similar, but at a lower magnitude, since water in the soil pore space increases the absorption of light (Drury 1993). Soil reflectance is also influenced by soil texture, surface roughness, the presence of minerals such as iron oxides, and organic matter. Some of these factors are inter-related, for example soil moisture is influenced by soil texture. Well drained soils, such as sands, will have higher reflectance values than poorly drained soils (Lillesand and Kiefer 1994). The mineral constituents are also important, since individual minerals have specific absorption bands associated with them. However, for many minerals the spectral resolution of Landsat TM bands is too coarse to detect these absorption bands (Lillesand and Kiefer 1994). Many bands appear only in the thermal part of the spectrum (Drury 1993) and are not of concern here.

In many instances the soil is partially or totally covered with vegetation so that the natural spectral signature will be a composite of the vegetation and underlying material. In

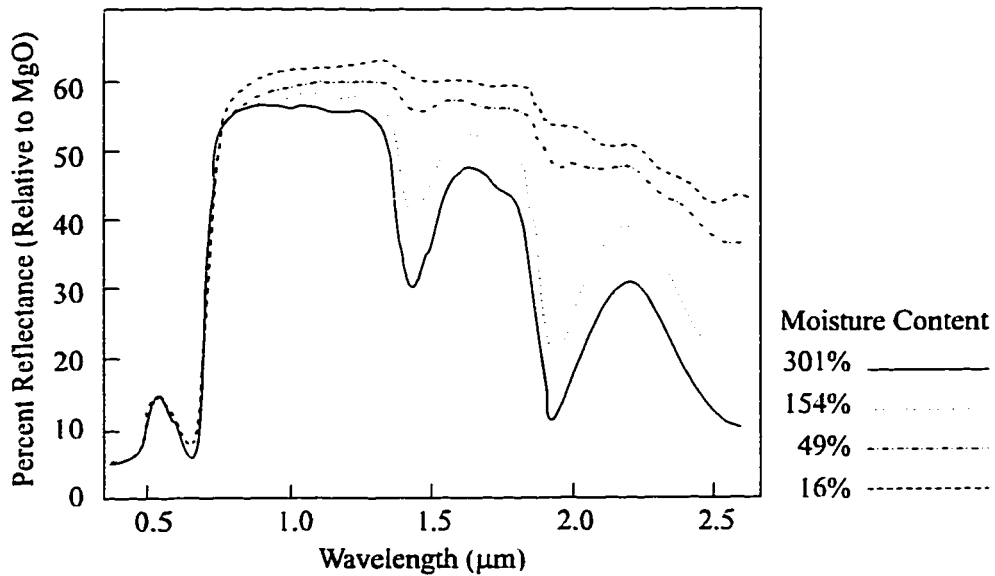


Figure 2-3. Changes in spectral response of a sycamore leaf in response to varying moisture content. After Elachi (1987).

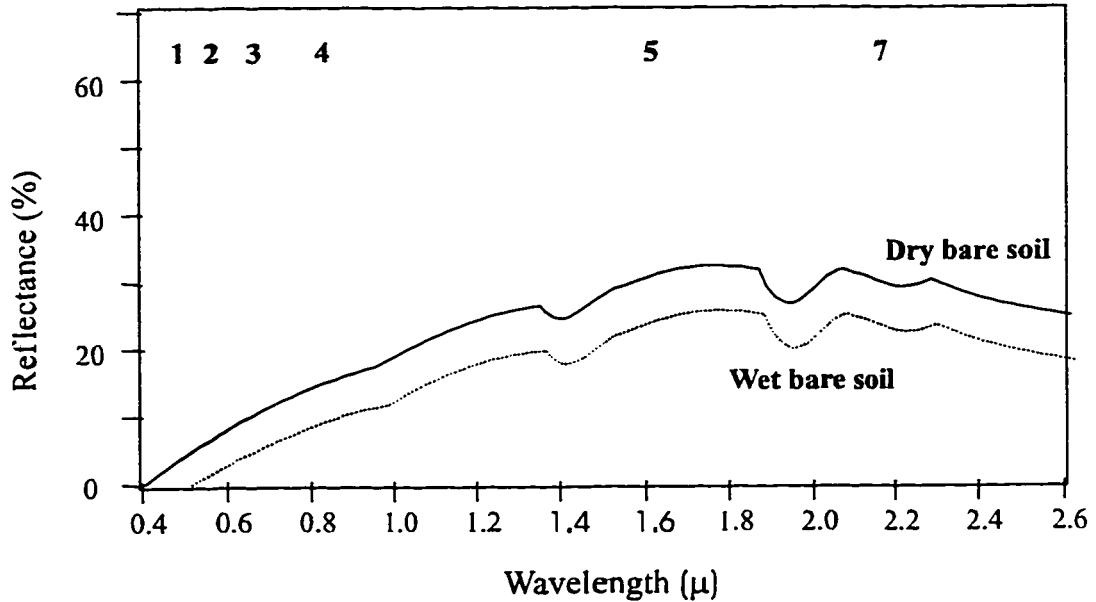


Figure 2-4. Generalized reflectance curves for dry and wet soils. Landsat TM bands are included for comparison. After Drury (1993) and Lillesand and Kiefer (1994).

general, when vegetation cover is less than 30 per cent, the signal received by the satellite will be dominated by that due to the reflectance from the soil. Once the vegetation cover exceeds 30 per cent the signal received by the satellite is that which would be expected by vegetation alone (Tueller 1987).

Mapping Aeolian Deposits using Satellite Images

The morphological characteristics of aeolian deposits, especially dunes, and differences in vegetation between dunes and inter-dune corridors makes it possible to identify and map these features using Landsat TM imagery (Marrs and Gaylord 1982; Jacobberger and Hooper 1991; Dwivedi et al. 1992; Goosens et al. 1993). Early work in this area was done by Breed and Grow (1979) and Breed et al. (1979) when regional surveys of several sand seas were conducted based on interpretation and mapping of Landsat imagery. Dune forms were classified based on shape and slip face orientation and measurements of length, width, and frequency were made to show the distribution of dune sizes within a region, and to show variety within dunes of the same type at different geographic locations. Other studies, such as work by Marrs and Gaylord (1982) and Kolm (1982) on the Ferris - Seminoe dune field, Wyoming, used Landsat Multispectral scanner (MSS) imagery for preliminary mapping and classification of aeolian land forms. Their results yielded qualitative information about dominant wind direction, pattern, and energy potential which, in conjunction with meteorological data gathered in the field, was used to generate models predicting wind characteristics in other parts of Wyoming (Kolm 1982).

Blount et al. (1990) used Landsat Thematic Mapper (TM) imagery to map sand provenance areas, transportation routes, and deposition sites in the Grand Desierto, Mexico. Comparisons made between lab spectra of samples taken from the field and satellite imagery indicated that variations in grain composition and coatings could be identified in TM imagery which allowed the provenance of the sands to be identified. In addition, areas of active and inactive sand were easily distinguishable. The results were

used to assist in interpretation of Quaternary events for the Gran Desierto region (Blount et al. 1990). In a similar study, Paisley et al. (1991) used Landsat data to discriminate between active and inactive sands, and to map aeolian activity in the Kelso dune field in the Mojave Desert, California. Active sand was found to have a higher reflectance in the visible and near infrared TM bands compared to inactive sands. Grain size measurements taken from samples in the field revealed that active sands tended to have more saltation sized particles (125 μm - 250 μm) predominantly consisting of quartz. Inactive sands contained the finer and coarser sediments, with a higher concentration of the heavier, dark, mafic minerals which have lower reflectance than quartz in the visible and NIR spectrum (Paisley et al. 1991; Rivard, personal communication). Based upon these differences in spectral reflectance, classes of varying degrees of sand activity were defined.

Detecting Change in Aeolian Environments using Satellite Imagery

Recent concerns about global warming and land use issues in arid regions has resulted in a strong interest (Blount et al. 1990; Paisley et al. 1991; Kaushalya 1992; Dwivedi et al. 1993; Chavez and MacKinnon 1994) in the potential of using satellite imagery for monitoring the affects of drought or mismanagement in these regions. The repeat coverage of satellite imagery, and the synoptic coverage it provides, make it a practical way of monitoring these often remote areas. Change detection uses multitemporal data sets (imagery acquired of the same area but for different dates) to discriminate areas of land cover change which have occurred over the selected period (Lillesand and Kiefer 1994). Areas of change can be identified by visually comparing images acquired for the different dates. More automated procedures, used for example by Robinove et al. (1981), demonstrated that land degradation in south western Utah was accompanied by an increase in albedo, which is the integral of light reflected by a feature relative to the integral of light incident upon it (usually from 0.15-4.0 μm). By combining reflectance values for each of the wavelength bands into a single image representing albedo, and differencing albedo images from different years, Robinove et al. (1981) were

able to detect and map relative changes in albedo due to degradation of the vegetation cover and to correlate these changes with levels of antecedent precipitation.

With the exception of occasional blowouts, dune deposits in Alberta are stabilized by vegetation. Changes that occur in the vegetation cover due to variations in soil moisture availability may provide some insight as to these dune's response to drought, and perhaps to climatic changes. These contrasts would be best exhibited by comparing wet year to dry year imagery (Drury 1993).

Chavez and MacKinnon (1994) compared vegetation differences over a wet year and a dry year using satellite imagery acquired for Yuma, Arizona. They found that a selective principal components procedure, where only two bands were used as input at one time, was effective at highlighting changes in vegetation between the two years. Information common to both images was mapped to the first principal component (PC) while information unique to either image was mapped to the second PC, thus emphasizing change between dates. They also compared the accuracy of using the Normalized Difference Vegetation Index (NDVI), which is sensitive to the amount of green vegetation present in a scene, versus the red band in determining changes in vegetation. They found that in arid regions where vegetation cover is not dense, there was not sufficient spectral contrast between the red and infrared reflectance of vegetation and soils to provide adequate separation using the NDVI. The high infrared reflectance of underlying soils biased the results of the NDVI ratio; whereas a radiometrically calibrated red band provided sufficient contrast to highlight changes that occurred from year to year, since vegetation has low spectral reflectance in the red band, the soil in their study had relatively high reflectance in this band (Chavez and MacKinnon 1994).

In a similar study, differences between wet season and dry season imagery was used as a means of assessing the influence of geomorphology on the distribution of vegetation on stabilized dunes in the Tsodilo Hills, Botswana (Jacobberger and Hooper 1991). Dune forms were visible on satellite imagery because of differences in vegetation composition between dune crests, interdune corridors, and the sand plains. Calculations of the NDVI for the images showed that the dune crests showed the highest seasonal

ranges of NDVI, followed by the corridors, and finally the plains. The results suggested that a causal relationship existed between the NDVI values, moisture availability, and the underlying geomorphology (Jacobberger and Hooper 1991). It was felt that similar relationships might be seen in the Rolling Hills area.

Rather than compare individual images acquired at different times, it is possible to process all of the temporal imagery to isolate cover types. For instance, the use of multi-temporal images captures phenological changes which occur in vegetation over the course of a season. These changes are then useful in more accurately distinguishing between cover types. Franklin (1991) used a principal component transformation of wet season - dry season imagery of the Sahel to distinguish between areas of annual grass growth and areas of woody cover. The wet season - dry season imagery provided the maximum amount of phenological and spectral contrast between wood and herbaceous vegetation, since the herbaceous layer was dormant during the dry season (Franklin 1991). The principal components were then used in an unsupervised classification routine in lieu of the individual bands to produce the final thematic map, which was then compared to air photographs to assess the accuracy of the classification (Franklin 1991). A similar investigation was done by Murphy (1996). Wet year and dry year Landsat imagery was acquired for the Duchess dune field in southern Alberta. A principal components analysis was performed on all bands simultaneously, and then selected components were used to generate colour composite images of the dune area. Murphy (1996) found that although most of the variance was contained in the first three PCs, a composite generated from PC 4, 5 and 6 was best at separating areas of aeolian deposits from non-aeolian deposits.

Conclusion

A considerable amount of research has been devoted to the development of techniques applicable to monitoring environmental changes in arid and semiarid regions. Although these studies were conducted in widely separated areas, there are sufficient

similarities between many of these regions and southern Alberta to warrant the application of these techniques to Alberta's dune fields.

CHAPTER 3

SITE DESCRIPTION

Location and Description of Study Area

The study area is in the Rolling Hills of southern Alberta (NTS map sheets 72L4 and 5). It extends from 111° 36' W to 111° 57' W and from 50° 13' N to 50° 22' N, covering an area of approximately 400 km² (Figure 3-1). The topography is flat to gently rolling, with an average elevation of ca. 750 m asl. Its form is principally controlled by the underlying, horizontally bedded, Late Cretaceous units, primarily the Oldman Formation, which consists of poorly consolidated marine and terrestrial sedimentary rock (Mossop and Shetsen 1994; Paterson 1996). Mantling these rocks are Late Wisconsinan glacial, glaciofluvial, and glaciolacustrine materials, consisting of moderately to well sorted sands and gravels in outwash plains, fans, deltas, and eskers (Shetsen 1987; Lemmen 1996). In the western portion of the study area lie the Rolling Hills, which reach a maximum elevation of 811 m asl. The hills, which are situated at the terminus of a 80 km long, north-south trending glacial flute complex, consist of sands and gravels associated with glaciofluvial deltaic deposits which were deposited into Glacial Lake Tilley (Shetsen 1987; Paterson 1996). After Glacial Lake Tilley drained, sometime between 17 ka BP and 11.2 ka BP (Christiansen 1979; Bryan et al. 1987; Vreeken 1989; 1993), these finer grained materials were preferentially deflated and deposited eastwards by prevailing winds as parabolic dunes, stringers and sand sheets (Figure 3-2).

Aeolian deposits in the area form a west-southwest to east-northeast trending belt approximately 3.5 km across at its widest point, and up to 5m deep (Roesler 1995). The deposits narrow and thin in an easterly direction. The entire field consists of one main

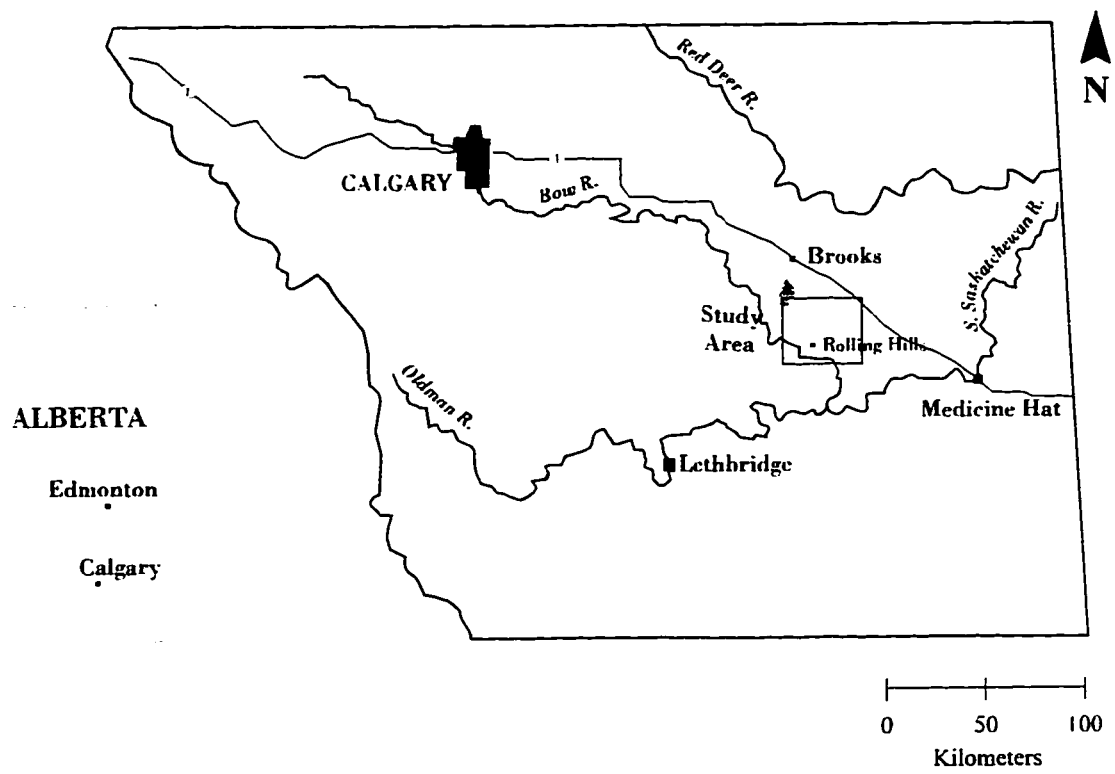
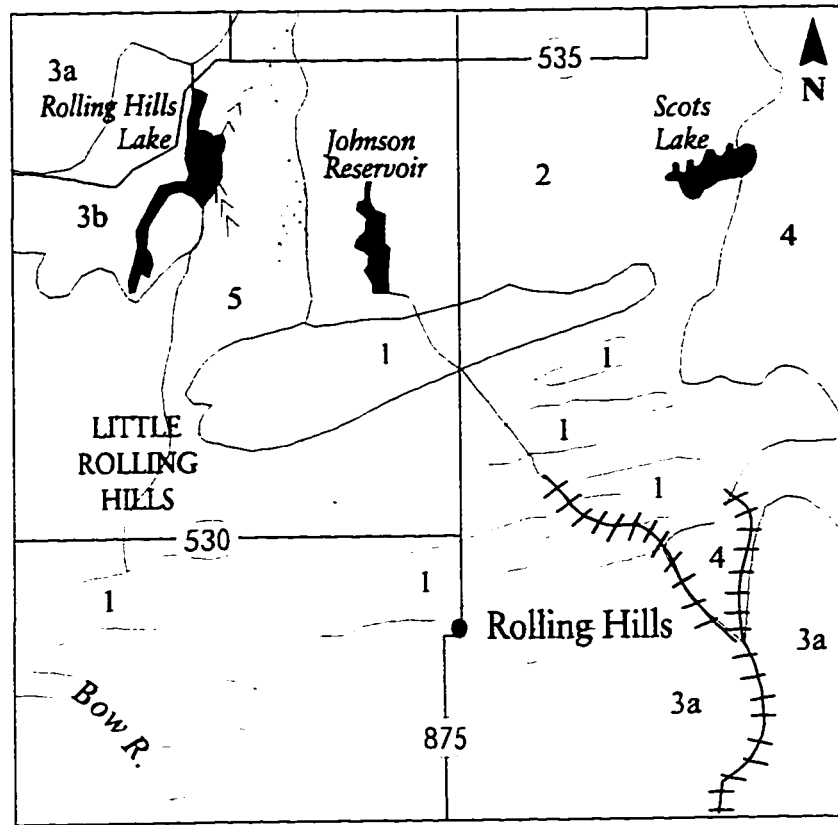


Figure 3-1. Location of the Rolling Hills dune field.



Scale: 1: 200 000


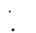
- 1 Aeolian deposits - parabolic and longitudinal dunes, with some blowouts; undulating to rolling topography; fine to medium grained sands and silts, up to 7m thick.
 - 2 Coarse sediments - sands and silts, in some instances modified by wind; undulating surface.
 - 3a Undulating topography with local relief of less than 3m.
 - 3b Hummocky topography with local relief of 3-10m.
 - 4 Draped moraine deposits - even thickness of till; some indications of minor water sorting; flat to undulating surface mirroring the topography of underlying bedrock.
 - 5 Ice contact lacustrine and fluvial deposits - gravel, sand, silts, and clay up to 25m thick; deposited in proglacial or supraglacial lakes and streams; undulating to hummocky topography.
 - 6 Bow River Valley
-  Minor Meltwater Channel
  Eskers

Figure 3-2. Surficial geology of the Rolling Hills region. Based on Shetsen (1987).

dune tongue approximately 21.69 km² in size and several smaller tongues with sand sheets present at the tongue margins and between dune fields (See Figure 3-3 and Table 3-1). Nearly all of the dunes in the area are part of larger composite forms, mainly of the parabolic or "wet sand" dune association (David 1977; 1988; 1993). Measurements of individual dunes by Roesler (1995) revealed that the average relief of the dunes was less than 3 m, with some individual dunes having local relief of 5 m. Many of the dunes measured had large areal extent (i.e. 400 m in length and 100 m wide) but had maximum relief of less than 3 m. In many of the larger dunes, dune-track ridges are discernable (see Figure 3-4). These are low, transverse ridges of sand that occur across the dune deflation area. They mark the position of former back slopes, where the base has been stabilized by vegetation or salt crusts. The dune continues to migrate, leaving these vegetated remnants behind as the dune-track ridge (David 1977; 1988; 1993).

Vegetation and Soils

The study area is part of the dry mixed grass ecoregion within the Eastern Alberta Plains (Strong 1992). Vegetation cover consists of species adapted to late summer aridity; mainly cool season, low growing perennials which become dormant or have completed their life cycle by July, when the greatest moisture deficits exist (Coupland 1952; Strong 1992; Kerr et al. 1993; Vance 1996). Dominant grasses include Needle-and-Thread (*Stipa comata*), Porcupine (*S. spartea*), Blue grama (*Bouteloua gracilis*), Western wheat grass (*Agropyron smithii*), Northern wheat grass (*A. dasystachyum*) and June grass (*Koeleria macrantha*) (Coupland 1950; 1952; 1960; Kerr et al. 1993). Principle forbs include Pasture sage (*Artemisia frigida*), Hood's phlox (*Phlox hoodii*) and Club moss (*Selaginella densa*), while Silver sagebrush (*Artemisia cana*), Shrubby cinquefoil (*Potentilla fruticosa*), and Alberta wild rose (*Rosa woodsii*) are the most frequently occurring shrubs (Coupland 1950; 1952; 1960; Kerr et al. 1993). Xerophytic plants such as Prickly pear (*Opuntia polyacantha*) and Cushion cacti (*Coryphantha vivipara*) are also relatively common in the area (Strong 1992; Looman 1983). In the

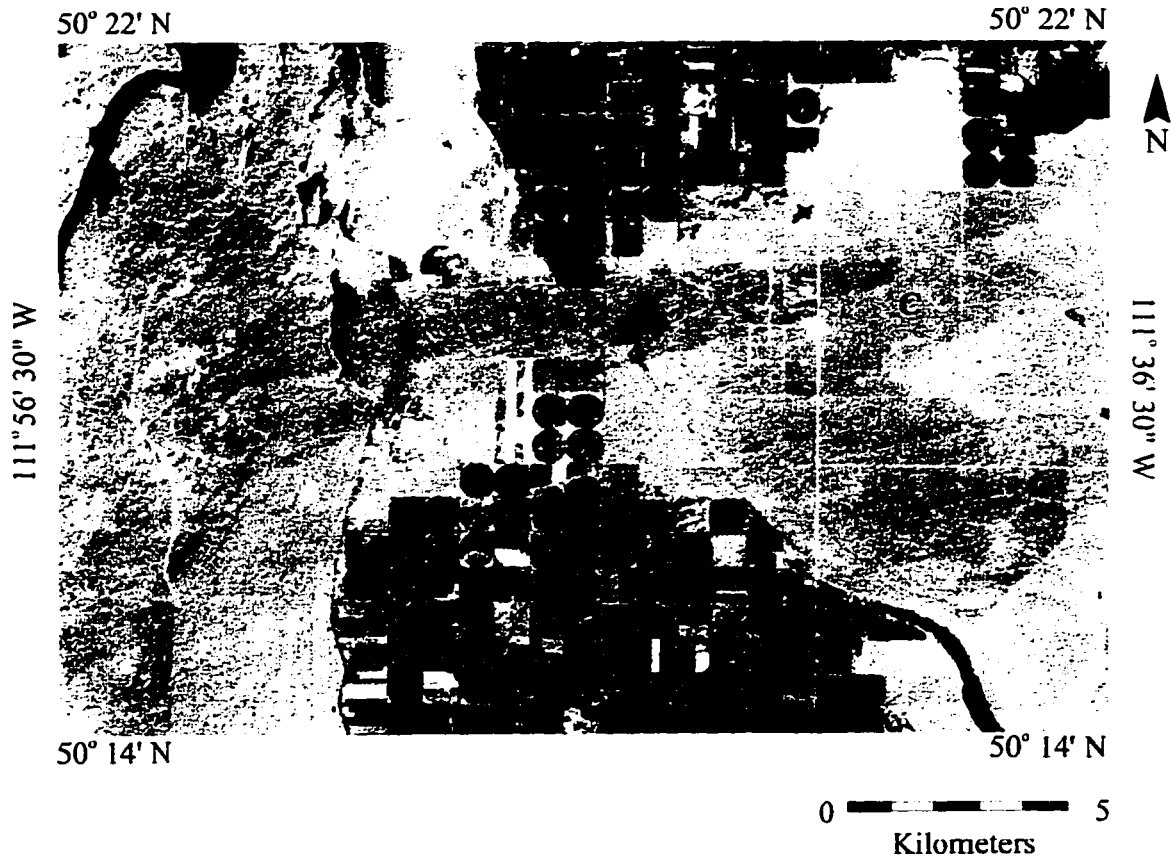


Figure 3-3. Colour infrared composite of the Rolling Hills area, created by assigning band 5 to blue, band 3 to green and band 4 to red. Area A corresponds with the main dune field, B corresponds with a minor dune area, and C corresponds with sand sheets. Landsat image acquired July 31, 1986.

Table 3-1. Spectral Interpretation of Features in the Rolling Hills Colour Composite shown in Figure 3-3

Feature	Composite Colour Tone	Radiation Characteristics
Water	Dark blue-black	Little or no radiation reflected.
Agricultural crops, healthy vegetation	Red	High near-infrared reflectance, with low red and mid-infrared reflectance.
Rangeland (including dunes and sand sheets)	Cyan to greenish cyan	Varying amounts of red and mid-infrared reflectance, with little near-infrared reflectance.
Roads, soil	White	High reflectance in all bands.

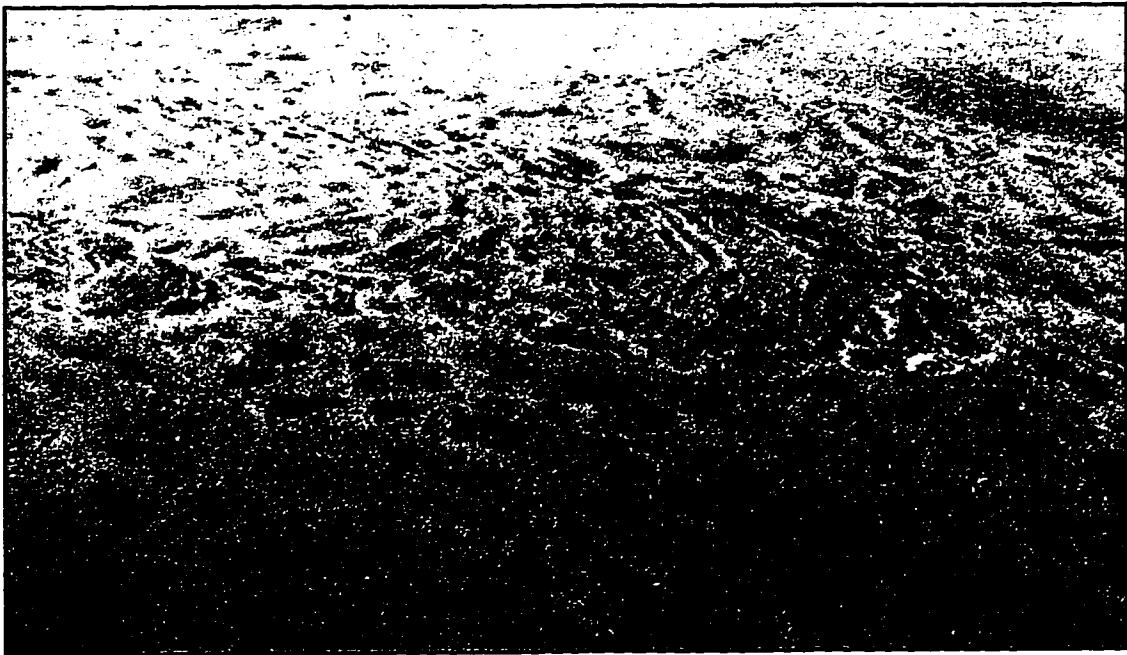


Figure 3-4. Oblique aerial photograph of a parabolic dune in the main dune area, with dune-track ridges clearly visible. These ridges mark former positions of the dune base. Photo taken on June 14, 1996.

Rolling Hills area growth on the plains tends to be dominated by grasses and Club moss (Figure 3-5), whereas growth on many of the sand dunes is dominated by low shrubs and forbs (Figure 3-6). Shallow dune deposits, especially in the eastern portion of the study area tend to be grass covered.

Species composition is dynamic and complex, varying as a function of differences in soil condition, topography and grazing pressure (Kerr et al. 1993). For example *Stipa spp.* tend to be dominant in areas of undulating topography, medium textured soil, or on intermediate slope positions (Coupland 1950; 1952; 1961). Where conditions are less favourable for *Stipa spp.*, such as upper slopes, or areas of finer or coarser soils, *Bouteloua spp.* emerge as the dominant species. *Bouteloua* have shallow branched root systems which allow them to utilize moisture near the surface. Higher levels of runoff associated with fine grained soils or rolling topography inhibits water penetration into the soil, favouring the development of short grasses over mid grasses (Coupland 1950; 1952; 1960). Rainfall easily infiltrates into coarse grained soils, and is quickly absorbed by shallow rooted species such as *Bouteloua*, but moisture which percolates to greater depth is not sufficient for the development of mid grasses such as *Stipa spp.* (Coupland 1950; 1952; 1960). Where moisture levels are adequate, in depressions or on lower slopes, *Agropyron spp.* replace *Bouteloua spp.* as the dominant species (Coupland 1950; 1952; 1960).

The greatest proportion of forbs and shrubs tend to occur in areas where moisture levels are higher or in areas with coarser soils, such as sand dunes (Coupland 1950; 1952; 1961). These plants have long tap roots which enable them to reach moisture reserves which have accumulated at depth. Higher moisture levels in sand deposits are due to reduced runoff, increased infiltration and decreased moisture lost via evaporation, leaving more moisture available for plant use (Coupland 1961). In addition, in the Rolling Hills region the aeolian landscape is superimposed on a former glacial lake bed. Fine grained glaciolacustrine deposits are an effective barrier preventing moisture from infiltrating to deeper levels.



Figure 3-5. Typical vegetation of the grassland plains. Species shown include Needle-and-thread and Blue grama grass with scattered patches of Pasture sage. Photo taken on July 3, 1996.



Figure 3-6. Typical vegetation in the Rolling Hills dune field. Species shown include Silver sagebrush, Pasture sage, Alberta wild rose, and Shrubby cinquefoil. Photo taken on July 3, 1996.

Species composition has been altered due the grazing of cattle, which is the primary land use of the region. Grazing of needle grasses tends to favor the abundance of blue grama (Coupland 1950; 1952; 1961; Kerr et al. 1993). Other species, such as pasture sage are also relatively abundant, and can serve as indicators of overgrazing in a region. This plant has low palatability for livestock, produces a high number of viable seeds, is drought resistant and easily invades areas depleted of grass cover (Looman 1983). Other primary land uses include cereal crop production, made possible through irrigation and strip farming practices, and sites associated with energy resource development (pipelines, well heads, etc.).

Soil development in the Rolling Hills region is characteristic of the Chernozemic order with Light Brown Chernozemic soils predominating and lesser amounts of Solodized Solonetzic soils occurring primarily in the central and eastern portion of the area (Kjearsgaard et al. 1983). Sand dunes are classified as Regosols since there is little evidence of profile development (Kjearsgaard et al. 1983). The most important soil series within these larger orders are those associated with the aeolian deposits, namely the Antelope, Vendisant, and Cavendish series. In Newell County these soil series are always associated with each other and represent the transition from sand dune to interdune areas (Kjearsgaard et al. 1983). The Antelope series is an Orthic Regosol, consisting of rapidly drained sands and occupying the most severe slopes in the dune areas (Kjearsgaard et al. 1983). Vendisant soils are classed as Rego Brown Chernozems, consisting of rapidly drained, loamy sands and showing weak profile development (Kjearsgaard et al. 1983). The Vendisant series tends to occur in the lower dune slopes occupying an intermediate landscape position between the Antelope and Cavendish series (Kjearsgaard et al. 1983). The Cavendish series consists of rapidly drained loamy sands and is classed as an Orthic Brown Chernozem (Kjearsgaard et al. 1983). Other minor series include the Rolling Hills series, a Brown Solodized Solonetzic soil comprised of well drained loamy sands, and the Island series, a Rego Gleyosolic soil associated with poorly drained areas within the aeolian deposits (Kjearsgaard et al. 1983).

Present Climate

Present day climate of the southern Alberta prairies in general can be characterized as having low levels of precipitation, cold winters and short, warm summers. This is primarily a function of fluctuations in the location of the subarctic jet stream. During the summer months, the jet stream is at its most northerly position, allowing for the influx of warm, moist Pacific air masses into the prairies. However much of the moisture contained in these air masses may be lost as the air crosses the Cordillera. During the winter months the jet stream moves to a more southerly position, allowing cold, dry Arctic air masses to move into the prairies, and preventing incursions of Pacific air (Gullet and Skinner 1992; Vance and Wolfe 1996).

Climate data collected at Brooks, approximately 40 km north of the study site, for the years 1961 to 1990, indicate that the mean annual temperature was 4.1°C, with July and August being the hottest months (average daily maximum temperature of 25.9° C), and January being the coldest month (-18.1° C). Annual precipitation for this same period was approximately 340 mm, with typically 60 per cent of the total annual precipitation occurring during the summer months, especially during June (Environment Canada 1993). Most precipitation falls in the form of rain, with snow accounting for only 30 per cent of the yearly amount. Wind speed data collected at Brooks indicates average winds of between 17-20 km/h, predominantly from the west or southwest. However maximum monthly wind speeds ranged from 77 to 87 km/h, with the highest winds occurring during the month of July and originating from the west or southwest (Environment Canada 1993). These strong winds when combined with long, warm days result in highly evaporative conditions, so that evapotranspiration usually exceeds annual precipitation (Skinner and Gullet 1992).

Climatic data collected since the late 19th century show that the prairie's have experienced several periods of warming and cooling. In general, the prairie regions experienced a gradual warming trend from 1890 to the 1940s followed by cooling which continued until the 1970s. Another warming period followed, lasting until the early

1990s. Climate data gathered from stations distributed throughout the prairies show that the 1980s were the warmest decade on record, with 1981, 1987, and 1988 being the first, second and tenth warmest years on record (Gullet and Skinner 1992). Mean annual temperatures for 1986, 1987 and 1988 were 5.57, 7.08 and 6.20°C respectively, which were from 1.47 to 2.98 degrees warmer than normal. Annual precipitation during these same years amounted to 387.6 mm, 277.9 mm and 250.3 mm respectively. In fact, during 1987 and 1988, potential evapotranspiration exceeded mean annual precipitation by about 60%, rivaling 1937 and 1938 as the driest years recorded (Vance and Wolfe 1996).

Conclusion

The dunes of the Rolling Hills dune field are believed to have formed during the Holocene (David 1979; 1993); the presence of multiple dune-track ridges suggests that the dunes have been active at various times. At present these dunes are stabilized by vegetation, but under the right conditions, i.e. increased prolonged aridity due to global warming or other local disturbances, these dunes could potentially be reactivated. The following chapters will discuss the methods used to delineate these aeolian sand deposits from their surrounding features and examine the potential for assessing climate-induced variations in these deposits.

CHAPTER 4

IMAGE SELECTION AND DATA PREPROCESSING

Introduction

Multi-temporal comparisons of the Earth's surface is an important capability of remotely sensed data. It involves the comparison of multi-date imagery acquired for the period of interest. In the past, comparisons between the images was done visually but with digital data, more automated techniques are available (Drury 1993). Change detection routines require that the data must be corrected for geometric and radiometric distortions. Correction ensures that differences that are seen between image dates represent real change and not residual 'noise' that results from the images not being aligned or properly calibrated. The first part of this chapter concerns the process of selecting the imagery used in this study and the corrections which were applied prior to further analysis. The remainder of this chapter focuses on the steps which were taken to generate a Digital Elevation Model (DEM) of the Rolling Hills area. The basis for creating the DEM was a digital contour map, generously provided by the Eastern Irrigation District (Porter 1995). This 1 m contour map represents the most detailed relief information available for the region. It was hoped that the DEM would provide a detailed topographic image of the Rolling Hills dune field which would be useful in identifying dune forms.

Image Selection

The main objective of this research was to differentiate between aeolian and non-aeolian deposits, based primarily on differences in soil moisture, and to determine whether any changes were discernable in these deposits between a wet and dry year. These soil moisture variations are manifested as differences in vegetation vigor and/or species composition between the deposits, for example, the tendency for the sand dunes to be dominated by small shrubs like wild rose. Thus it was necessary to select remotely sensed data which would best differentiate vegetation. Landsat Thematic Mapper (TM) imagery was chosen because the resolution, wavelength range, and spectral bands of this sensor were designed to improve vegetation differentiation (Lillesand and Kiefer 1994). TM band 4, for instance, is centered on a region of maximum spectral sensitivity to plant vigor. Plant water stress is most easily detected in TM bands 5 and 7 (Lillesand and Kiefer 1994). Table 4-1 lists the seven TM spectral bands and briefly summarizes the principal application of each. Although Landsat TM is well suited for detecting vegetation, there is a high degree of correlation between the TM image bands leading to some degree of redundancy in the information content. Not all bands may be appropriate or useful for a particular application. For example, Murphy's (1996) work on the Duchess dune field, 75 km north of the study area, demonstrated that most of the variance, and thus the greatest information content in the scenes, was accounted for in TM bands 3, 4 and 5. Accordingly it was felt that bands 3, 4 and 5 for both years would be sufficient for this study.

Determining which years were considered wet or dry followed Proudfoot's (1994) work on drought patterns in the Medicine Hat area about 100 km southeast of the Rolling Hills region. Departures from mean annual precipitation (Figure 4-1) show that 1988 was one of the driest years between 1961 and 1990 while 1986 was the wettest year. Based on this information, the Landsat TM image archives were searched for cloud free summer coverage of the Rolling Hill region for the years 1986 and 1988. To minimize

Table 4-1. Thematic Mapper Spectral Bands. After Lillesand and Kiefer (1994)

Band	Location (μm)	Nominal Spectral Wavelength	Principle Applications
1	0.45-0.52	Blue	Water penetration, soil/vegetation discrimination, cultural features.
2	0.52-0.60	Green	Peak green reflectance for vegetation discrimination, cultural features.
3	0.63-0.69	Red	Chlorophyll absorption region for plant discrimination, cultural features.
4	0.76-0.90	Near infrared	Determining vegetation type, vigor and biomass content, soils moisture, and delineating water bodies.
5	1.55-1.75	Mid-infrared	Vegetation moisture content, soil moisture, and separating snow from clouds.
6	10.4-12.5	Thermal infrared	Vegetation stress analysis, soil moisture, and thermal mapping.
7	2.08-2.35	Mid-infrared	Mineral and rock types, vegetation moisture content.

changes in reflectance due to differences in the solar elevation and azimuth, anniversary date images were sought; that is, images acquired for close to the same date but in different years. Imagery acquired on July 31, 1986 and July 20, 1988 met these requirements. Table 4-2 summarizes the image specifications.

Image Correction and Rectification

All satellite imagery contains some degree of radiometric and geometric error. These errors must be corrected, especially when using multi-temporal data sets or change detection techniques. If left uncorrected, these distortions create 'noise' in the imagery

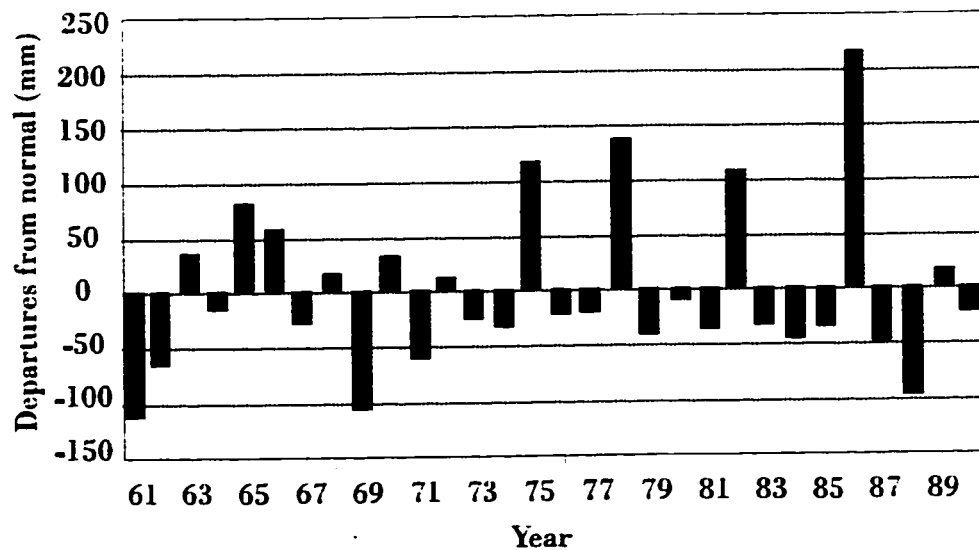


Figure 4-1. Departures from mean annual precipitation of the Medicine Hat region, 1961-1990. From Proudfoot (1994).

Table 4-2. Landsat TM Imagery Specifications for 1986 and 1988

Property	July 31, 1986	July 20, 1988
Product Number	95347802-01	95347801-01
Track and Frame Number	Track 40 Frame 25	Track 40 Frame 25
Satellite	Landsat 5	Landsat 5
Instrument	Thematic Mapper 10	Thematic Mapper 10
Bands	3, 4 & 5	3, 4, & 5
Corrections Applied	Systematic geocoded Radiometric calibrations	Systematic geocoded Radiometric calibrations
Scene Size	25 km subscene	25 km subscene
Scene Center	111° 46' 01" W 50° 11' 07" N	111° 46' 01" W 50° 11' 07" N
Pixel Resolution	25 m	25 m
Solar Elevation (degrees)	52	54
Solar Azimuth (degrees)	135	137
Cloud Cover (%)	0	0

that may be mistaken to represent changes that have occurred over the period of interest. Radiometric distortions are discrepancies in the measured brightness values of the pixels relative to the spectral reflectance of the ground, due to the behavior of the detectors and atmospheric effects (Richards 1986; Jensen 1986). Instrumentation errors are usually predictable and constant and are corrected before the imagery is distributed (Jensen 1986). Atmospheric distortions arise from the tendency for light to be scattered or absorbed by the atmosphere, depending upon its wavelength and atmospheric conditions. Shorter wavelengths are scattered by the atmosphere and the resulting image will be brighter relative to the actual brightness of the ground. Longer wavelengths (greater than 0.8 μm) tend to be absorbed by the atmosphere, primarily by water vapor, causing the data from these bands to be darker compared to actual reflectance by the ground (Jensen 1986).

There are many methods available to correct for atmospheric effects. The most sophisticated techniques require ground measurements acquired on the day of satellite image acquisition. These measurements provide a reference index of radiance for surface features, regardless of atmospheric conditions, which can then be used to calibrate the radiance values recorded at the satellite (Chavez 1989). These data were not available, so a simple image based technique known as haze removal or dark pixel subtraction was done; it uses the frequency histogram for each image band to identify the darkest pixel in the scene (Jensen 1986). These values usually occur in deep, clear water or deeply shadowed regions. Any reflectance emanating from these features is due to light which has been scattered by the atmosphere, since water absorbs most of the light incident upon it and shadowed areas are not receiving direct illumination (Jensen 1986). This pixel value is subtracted from every pixel in the scene, shifting the entire histogram to the left so that the lowest value in the scene is now at the origin of the histogram. Figure 4-2 illustrates the effect of scattering on bands 3 for the 1986 image and the resulting histogram after the haze removal technique was applied to all bands for 1986 and 1988, using the SCALAR routine in Idrisi (Eastman 1995). Table 4-3 shows the original and adjusted pixel values for each band. If the image had a minimum value of 0, no correction was applied. This

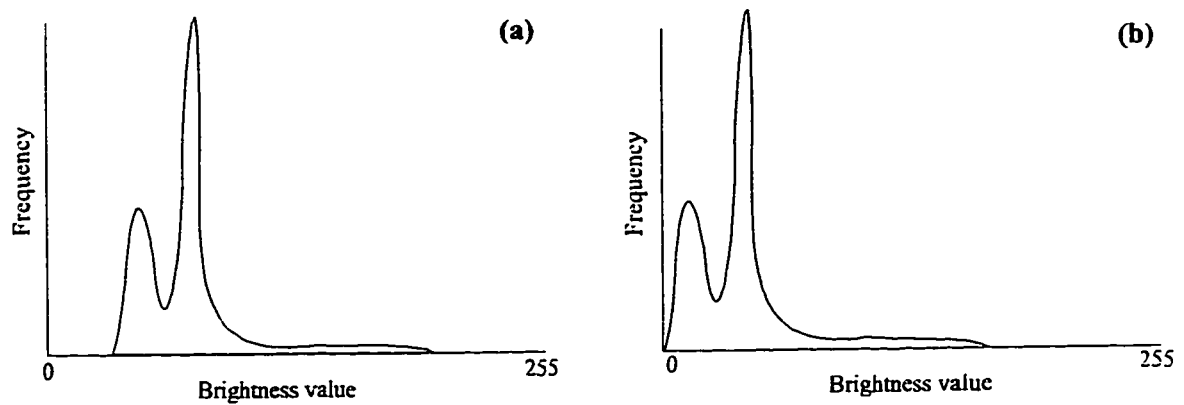


Figure 4-2. Illustration of the effects of atmospheric scattering on TM band 3 for 1986. (a) before correction, and (b) after correction.

Table 4-3. Digital Numbers used in Atmospheric Correction

Image Band	Original Min.	Original Max.	Adjusted Min.	Adjusted Max.
1986 -TM3	19	106	0	87
1986 -TM4	4	187	0	183
1986 -TM5	0	238	0	238
1988 -TM3	20	226	0	206
1988 -TM4	5	207	0	187
1988 -TM5	0	255	0	255

procedure removes first order atmospheric distortions, however multiplicative transmission effects were left uncorrected due to difficulties in effectively modeling the errors.

Geometric errors are due to movements of the scanner, satellite platform, and motion and curvature of the earth. Systematic errors (i.e. scan skew, scan velocity non-linearities, and panoramic distortion) are corrected before the image product is sold. However, non-systematic errors caused by roll, pitch, yaw, and altitude of the sensing platform may or may not be corrected prior to the imagery being distributed. If not corrected the imagery will be nonplanimetric, and will require correction using ground control points (GCPs), i.e. features whose location can be determined for both the image and a map (Jensen 1986; Richards 1986). This is known as geometric rectification and involves finding the mathematical relationship which exists between the location of a pixel in an image, and its corresponding coordinate location on a map. The two sets of coordinates are related through mapping functions of the general form:

$$x' = f(x,y)$$

$$y' = f(x,y)$$

where :

x and y are the coordinates taken from a map

x' and y' are the corresponding coordinates for the feature in the image.

Exact forms for these mapping functions are not known precisely, but the relationship can be defined by fitting a curve to the data using simple polynomial equations. Solving for the equation coefficients determines the nature of the coordinate transformation needed to relocate every pixel in the original input image to its proper position in the rectified output image (Jensen 1986). The pixel value at a particular location in the original image is then relocated to the appropriate location in the rectified image through intensity resampling.

For this study, GCPs were selected that could be easily identified on both images and a 1:50 000 scale map (NTS 72L4/5) of the area. The GCPs were spread throughout the image area and included road intersections, irrigation canals, airstrips, and water bodies which appeared to have remained stable over the 1986-1988 period. The image

coordinates and the corresponding UTM coordinates were recorded for each GCP and used as the input for a bilinear equation in Idrisi's RESAMPLE module (Eastman 1995). The root mean square errors (RMS) were calculated for each GCP. Generally, registration within 0.5 pixels is considered acceptable; any point with a greater amount of error was re-evaluated or omitted from the final calculation. In total, 18 GCPs were accepted in the final calculations and a nearest-neighbour resampling method was used to interpolate pixel intensities. Rather than do all subsequent analysis on the full image, a subset of the image was extracted from the full scene which contained all the features of interest. The final step was to convert the pixel digital numbers (DNs) to at-satellite radiance units ($W/steradian/m^2/\mu m$) to facilitate comparison between the two image sets. Appendix I lists the GCP coordinates used to register the imagery and the residual errors associated with each point. Equations used in the RADIANCE module of Idrisi (Eastman 1995) for converting DN's to radiance are provided in Appendix II.

Creating the Digital Elevation Model

The most detailed topographic data available for the Rolling Hills area was from a 1 m interval contour map of the Eastern Irrigation District (Porter 1994). It was felt that a DEM produced from the contour map would give a detailed picture of the topography of the Rolling Hills area. Comparing the DEM with the Landsat TM data may also have provided a means of assessing the ability of the satellite imagery to highlight dune forms.

Digital data was provided by the Eastern Irrigation District in DXF (Digital exchange file) format. The file was imported into Idrisi (Eastman 1995) for analysis. A subset of the region 13 km by 7.6 km in size, which included all of the dune areas, was extracted from the original scene to shorten the processing time and reduce the size of the final file. The contours were generalized to remove extraneous data points using FILTER (Hemenway 1992), a program developed in the Department of Earth and Atmospheric Sciences, University of Alberta. Several iterations were required to determine the proper radius distance for the filtering operation, but 30 m proved to be sufficient to remove all of

the unwanted data points. The filtered contour file was then used as the input into Q-SURF (Hemenway 1994) a surfacing program developed in the department which uses multi-quadric equations to generate a surface from contour lines. The pixel resolution was set at 8 m. Experimentation with other pixel sizes showed that with smaller pixels the quadric equation created features which were not part of the actual data set and with pixels greater than 12 m important details were lost.

To view the resulting DEM as a three dimensional model, a hillshade image was generated using the SURFACE module in Idrisi (Eastman 1995), with the solar azimuth and elevation set at 315° and 20° respectively. The resulting model appeared a uniform mid-gray colour and showed no land forms whatsoever. The frequency histogram for the image showed very little differentiation in the gray tones for the file and the image was contrast stretched to enhance the contrast. Even after applying a contrast stretch, the topography appeared so subdued that very little detail could be discerned. Most importantly, dune forms which could be seen in the raw contours were no longer visible in the DEM. Several attempts were made to improve the display by altering the solar azimuth and elevation, increasing the vertical exaggeration, and changing the stretch parameters. There was no improvement in the results.

The problems encountered in generating the DEM relate to the equation that was used to create the surface. A multi-quadric equation is an exact fitting equation and it interpolates smoothly between points, resulting in a smooth surface. In a region where there are no pronounced differences in relief the quadric equation may produce results that are too smooth and the features of interest are no longer visible. To counter this, a second attempt was made at generating the DEM, using the linear interpolation function in Idrisi's INTERCON module (Eastman 1995). This module employs a linear interpolation to create a surface from rasterized contours. An empty raster grid, 1659 columns by 951 rows with 8 m pixels was created using INITIAL (Eastman 1995) to accept the rasterized contours. The contours were converted using the LINERAS command (Eastman 1995). The new raster file was used to interpolate the surface using INTERCON (Eastman 1995) and a hillshade model was created in the same manner as previously discussed. The

resulting hillshade model was contrast stretched to enhance the image for display (refer to Appendix III).

The results obtained using linear interpolation were better than those obtained with the quadratic equation. The dunes were clearly visible, especially dunes in the main dune field. However, the equation introduced noise that was not present in the data. This noise consisted primarily of southeast trending, linear elements distributed throughout the scene. In addition, small depressions and mounds appeared as star shaped features. Several filtering techniques were applied, including low pass filters and directional filters, in an attempt to improve the image and remove at least some of the noise. The best results were obtained with a southeast directional gradient filter. The dune forms are oriented in a southeast trend through the scene and it was hoped that a directional filter would detect the dunes and eliminate the non-diagonal elements. This was successful in eliminating much of the noise, however the linear elements associated with the noise that were orientated in the same direction as the dunes, remained. The problem is likely associated with the algorithm used in the linear interpolation. Multiple scans are made through the data; horizontally, vertically, and diagonally. For each pass, for cells where the value is unknown, the interpolated elevation and the slope is stored. The value that is ultimately kept is the value which yielded the maximum slope (Eastman 1995). With some irregular shallow contours, the interpolated values may oscillate sharply, leading to dramatic changes in slope (Eastman 1995).

Conclusion

Radiometric corrections and geometric rectification are vital in change detection studies to ensure that the changes that emerge through time-comparison processing represent real change. Georectification of this image set was relatively straightforward due to the subdued topography in the area. Atmospheric distortions are more difficult to correct and the techniques used here are by far the simplest available. Fortunately, scattering is most problematic in the shorter, visible wavelengths (e.g. Landsat TM bands

1-3) which were either not used in this study, or the effects of scattering were removed. Unfortunately, the DEM proved to be not as effective as it was hoped in highlighting dunes in the Rolling Hills dune field. The two methods used to produce the DEM resulted in the final image being either too smooth, where the features of interest were lost, or in the final image being too noisy for further analysis.

CHAPTER 5

MULTI-TEMPORAL IMAGE PROCESSING

Introduction

There are several types of classification techniques commonly employed in remote sensing, including the parallelepiped, minimum distance to means, histogram peak selection, and maximum likelihood; all fall under the general headings of supervised and unsupervised classification. In supervised classification, the user selects training sites from the scene which are used to generate the statistics subsequently used to classify every pixel in the image. Training fields must represent homogeneous areas of cover, and every class present in the scene must be identified (Richards 1986; Drury 1993; Lillesand and Kiefer 1994). In unsupervised classification, pixels are assigned to different classes on the basis of their spectral properties (Drury 1993). Training fields are not defined by the analyst, rather the image is segmented into natural clusters based on the spectral information present in the imagery. The analyst then assigns category names to the resulting clusters (Richards 1986; Drury 1993; Lillesand and Kiefer 1994). This chapter will discuss the principles of cluster analysis, its application to multi-temporal image sets in this analysis, and the results that were obtained.

Cluster Analysis

Many clustering algorithms exist that can be used to segment the data in an unsupervised classification routine. A common technique known as K-means clustering or migrating means was used in this study (Richards 1986; Lillesand and Kiefer 1994). In K-means cluster analysis, the analyst specifies the initial number of clusters. The number of natural clusters present in the scene is not known, so this value is usually set quite high. The algorithm then arbitrarily 'seeds' the specified number of clusters in multidimensional space. The distances are calculated for each pixel to the cluster centroids and each pixel is assigned to the cluster whose mean vector is closest (Figure 5-1). After all the pixels have been assigned, the mean vectors are recalculated for each cluster and the image is classified again. This process continues until no significant changes occur in the location of the mean vectors between successive iterations (Davis 1986; Richards 1986; Lillesand and Kiefer 1994).

This technique is computationally intensive and is usually performed on subsets of the original data or training fields. To generate the training fields, the TRAIN module of Terra Firma (Eyton 1992) was used. TM bands 3, 4 and 5 for 1986, converted from DN's to radiance units, were used as input. Training fields were created using a systematic sampling method where pixels occurring in every tenth row and tenth column were included for analysis. Since the number of clusters in the scene was unknown, 40 clusters was specified for the initial iterations. Terra Firma generates statistics related to the separability of each cluster. This includes the mean distance and standard variation of each pixel in a cluster to its centroid and the F-ratio, which is the ratio of the between sample variance and the within sample variance (Davis 1986). The F-ratios were plotted versus the cluster numbers (Figure 5-2) to determine where peaks occurred in the distribution. These peaks represent the optimum number of clusters in the data, where the variance between samples is high while within sample variance is low (Davis 1986; Richards 1986). Several peaks occurred in the distribution. For ease of identifying the cover types, 15 was selected as the optimum number of clusters for 1986. The process

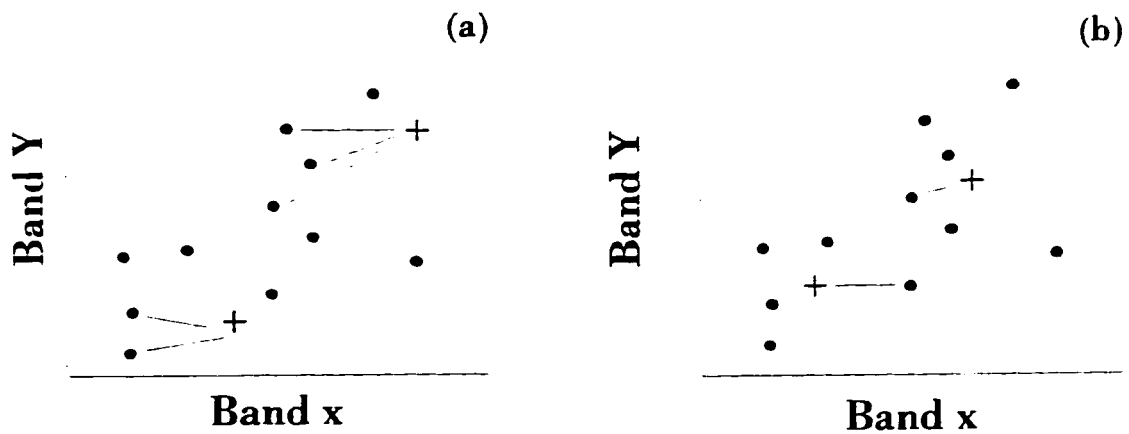


Figure 5-1. K-means or migrating means cluster analysis; (a) shows the initial 'seeding' of the mean vectors and the pixel assignment, (b) shows the result of the second iteration. The process continues until there is no significant change in the position of the mean vectors between iterations. After Richards (1986).

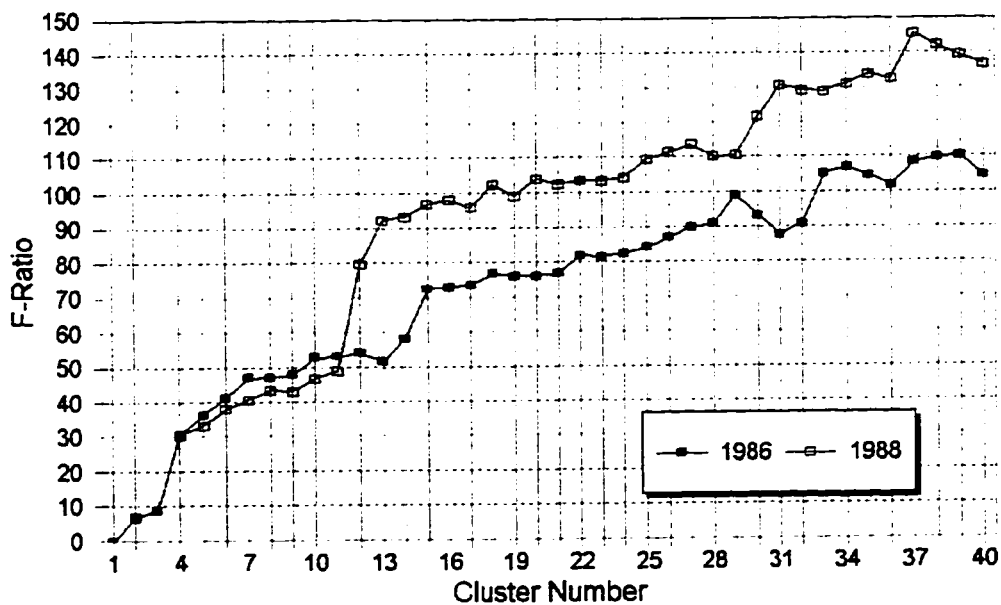


Figure 5-2. Plot of F-ratios versus cluster number. Peaks in the data indicate the number of clusters where the between sample variance is high while within sample variance is low.

was repeated using bands 3, 4 and 5 for 1988 with 16 clusters being selected as the optimum number. TRAIN was used again to generate training statistics for 15 and 16 clusters, for 1986 and 1988 respectively. The confusion matrices generated for the training fields indicated overall classification accuracies of 97.26 and 96.68 per cent, for 1986 and 1988, which showed that there was little spectral confusion between clusters. Both complete data sets were then classified using K-means cluster analysis, available in the CLASS module of Terra Firma (Eyton 1992). Legend categories were assigned to each class using air photos with a scale of 1:30 000 as a reference.

Once the classification was complete, the classes were further refined by examining each class individually. Those classes which fell within the agricultural areas were compared to colour infrared composites for the same year and grouped into two general agricultural classes, one which represented healthy crops, the second which corresponded with fallow fields. Non-agricultural areas were of the greatest concern in this study, and generalizing the agricultural areas into two classes would not jeopardize the classification of the other classes. This resulted in two final maps with eight spectral land cover classes. The areas of each spectral class were calculated using the AREA module in Idrisi (Eastman 1995) to determine whether there were differences in the classification results for the wet and dry year imagery.

At this stage a method was needed to define spectral change classes. Because the key concern was with the dune areas the dune classes were selected for further analysis. The first step was to generate two class masks, where the target class was isolated for each year. This was done using the RECLASS module in Idrisi (Eastman 1995). The 1986 classed image was reclassified so that dunes in 1986 had a new integer value of 1 while all other classes had a new value of 0. The same was done for the 1988 classed image, with the exception that dune pixels were assigned a value of 2. Using Idrisi's OVERLAY function (Eastman 1995), the new images were added together. This resulted in a three class change map for the dune areas. Those pixels which were classed as dunes in 1986 alone now had a value of 1, while those pixels classed as dunes in 1988 alone now had a value of 2. Pixels which were classed as dunes in both years now had a value of 3.

This provided a fuller picture of where differences between the two years occurred. For display purposes, the change classes were draped over the 1986 band 5 image.

Results of Image Classification

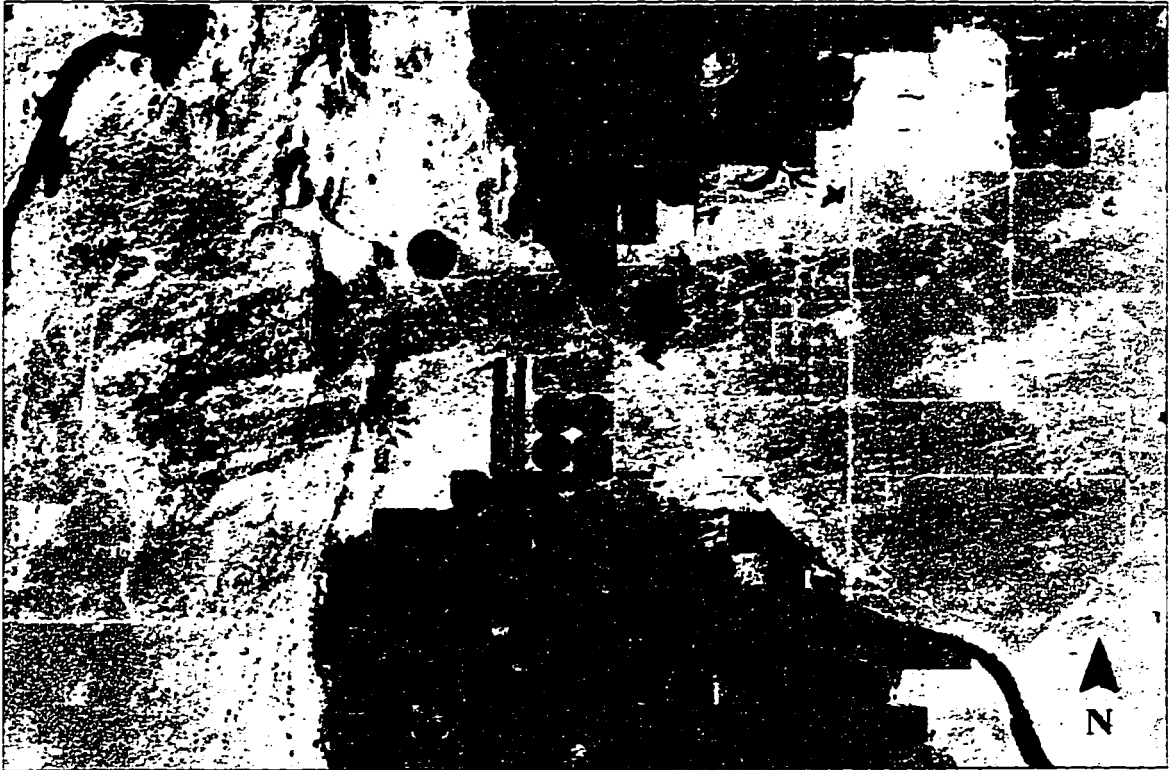
Using K-means cluster analysis, two spectral land cover maps were created (Figures 5-3 and 5-4). Area calculations based on these spectral classes are presented in Table 5-1, and indicate which classes experienced areal change due to spectral differences between the wet and dry years. To help explain the changes seen between the two years, the confusion matrices generated for the training fields for the K-means cluster analysis are shown in Table 5-2 and Table 5-3 and the reflectance curves for each band are shown in Figure 5-5. Finally, the image which highlights change classes in the dune deposits is shown in Figure 5-6.

Image Interpretation and Discussion

Examination of Figures 5-3 and 5-4 reveals definite differences between spectral classes for the two image dates. For example, parabolic dunes are clearly visible in the southeast portion of the 1986 image which are not visible in 1988. There are also regions in the Rolling Hills which were classed as dunes in the 1986 image and do not appear in the 1988 image. Dune deposits appear in the central parts of the 1988 scene which do not appear in the 1986 scene. Overall, Table 5-1 shows that areas classed as dunes are more extensive in the 1988 imagery. Sand sheets and the grassland classes had greater areal extent in the 1986 image, as did wetlands regions. Those areas labeled as soil and roads were more extensive in the 1988 image. These area measurements suggest that a great deal of spectral change has occurred between the image dates, but this can not be translated into actual change in the areal extent of the deposits themselves, i.e. that the dune field has expanded 15.47 km² in two years.









50° 22' N
111° 56' 30" W

50° 22' N
111° 36' 30" W



50°14' N
111° 56' 30" W

50°14' N
111° 36' 30" W

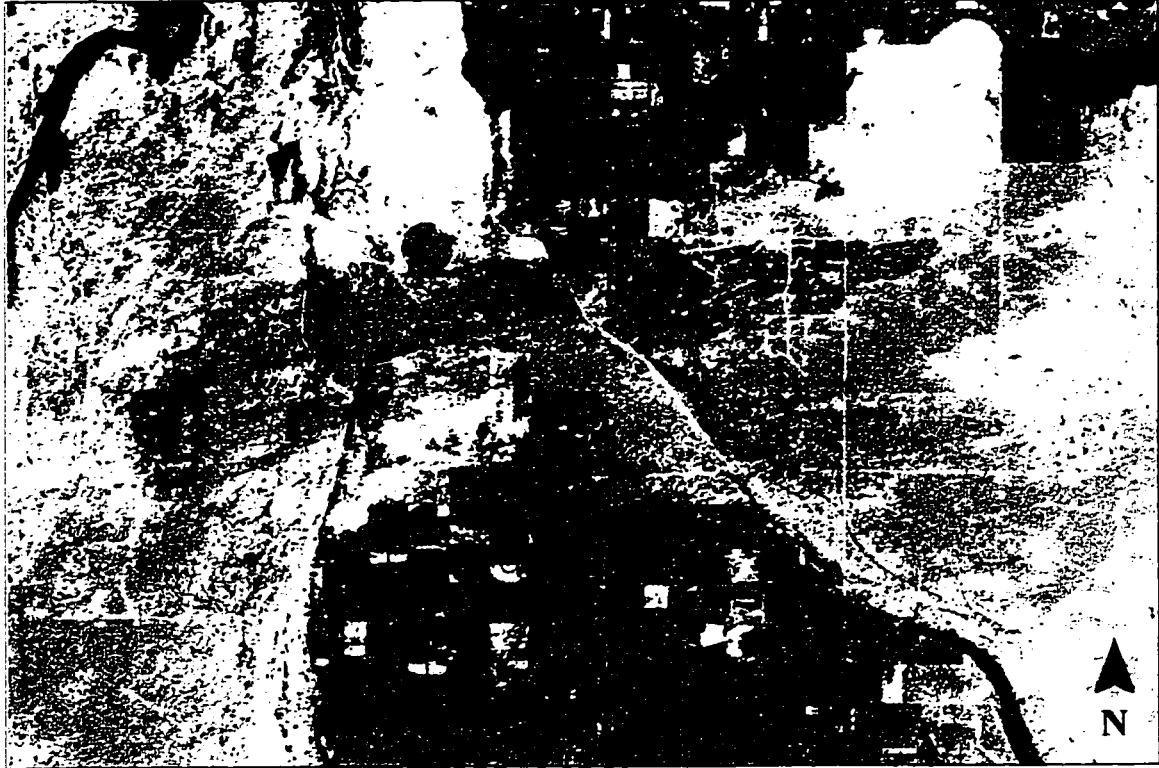
- | | |
|--|---|
|  Sand dunes or sand source areas associated with grasses and low shrubs |  Lakes and sloughs |
|  Sand sheets and interdune areas associated with grasses |  Wetlands / Irrigation canals |
|  Prairie grassland. |  Agricultural areas 1 |
|  Soil / Gravel roads / Irrigation canals |  Agricultural areas 2 |

Scale 1:200 000

Figure 5-3. Land cover map of the Rolling Hills dune field obtained through K-means cluster analysis of Landsat TM bands 3, 4 and 5 for 1986.









50° 22' N
111° 56' 30" W

50° 22' N
111° 36' 30" W



50° 14' N
111° 56' 30" W

50° 14' N
111° 36' 30" W

- | | |
|--|---|
|  Sand dunes or sand source areas associated with grasses and low shrubs |  Lakes and sloughs |
|  Sand sheets and interdune areas associated with grasses |  Wetlands / Irrigation canals |
|  Prairie grassland |  Agricultural areas 1 |
|  Soil / Gravel roads / Irrigation canals |  Agricultural areas 2 |

Scale 1:200 000

Figure 5-4. Land cover map of the Rolling Hills dune field based on K-means cluster analysis of Landsat TM bands 3, 4, and 5 for 1988.

Table 5-1. Area Comparison of Each Land Cover Class

Land Cover Class	1986 (km²)	1988 (km²)	Difference (km²)
Dunes	34.45	49.92	+15.47
Sand Sheets	97.25	73.01	-24.24
Prairie Grassland	99.09	89.03	-10.06
Bare Soil/Roads	30.27	54.34	+24.07
Lakes and Sloughs	7.82	7.47	0.35
Wetlands	12.61	7.60	-5.01
Agricultural 1	82.37	83.22	+0.85
Agricultural 2	22.54	21.81	-0.73
Total	386.40	386.40	

Table 5-2. Confusion Matrix for 1986 Cluster Analysis

	1	2	3	4	5	6	7	8	9	10	11	12	13	14	15
1	97.21	.00	.56	.00	.00	.56	.00	.00	.00	.00	.00	1.68	.00	.00	.00
2	.00	98.53	.00	.00	1.47	.00	.00	.00	.00	.00	.00	.00	.00	.00	.00
3	.75	.00	96.25	.00	.00	1.50	.00	.00	.00	.00	.00	.00	.00	.00	.00
4	.00	.00	.00	95.65	.00	.00	.99	.00	.00	.00	.06	.00	.31	.00	.00
5	.00	.68	.00	.00	96.60	2.72	.00	.00	.00	.00	.00	.00	.00	.00	.00
6	.29	.00	1.45	.00	.00	98.26	.00	.00	.00	.00	.00	.00	.00	.00	.00
7	.00	.00	.00	1.68	.00	.00	97.02	.00	.00	.00	.00	.56	.19	.00	.00
8	.00	.00	.00	.00	.00	.00	.00	97.85	.00	.00	.00	.00	.00	.00	2.15
9	.00	.00	.00	.00	.00	.00	.00	.00	100.0	.00	.00	.00	.00	.00	.00
10	.49	.00	2.46	.00	.00	.00	.49	.00	.00	96.06	.00	.49	.00	.00	.00
11	.00	.00	.00	.13	.00	.00	.50	.00	.00	.00	98.36	.06	.00	.00	.95
12	.00	.00	.00	.00	.00	.00	4.23	.00	.00	2.11	.70	92.96	.00	.00	.00
13	.00	.00	.00	.00	.00	.00	.00	.00	.00	.00	.00	.00	100.0	.00	.00
14	.00	.00	.00	.00	.00	.00	.00	.00	.00	.00	.00	.00	.00	100.0	.00
15	.00	.00	.00	.00	.00	.00	.00	1.90	.00	.00	8.67	.63	.00	.00	88.79

Over-all Correct Classification = 97.26 %

1-agricultural, 2-agricultural, 3-agricultural, 4-sand sheets, 5-agricultural, 6-agricultural, 7-sand dunes, 8-agricultural, 9-agricultural, 10-wetlands, 11-plains, 12-wetlands, 13-wetlands, 14-water, 15-bare soil, roads.

Table 5-3. Confusion Matrix for 1988 Cluster Analysis

	1	2	3	4	5	6	7	8	9	10	11	12	13	14	15	16
1	99.55	.00	.00	.00	.00	.00	.00	.00	.00	.00	.00	.00	.00	.00	.00	.45
2	.00	100.00	.00	.00	.00	.00	.00	.00	.00	.00	.00	.00	.00	.00	.00	.00
3	.00	.00	87.73	.00	1.84	.00	.00	.00	.61	.00	.00	.00	3.68	6.13	.00	.00
4	.00	.00	.00	100.00	.00	.00	.00	.00	.00	.00	.00	.00	.00	.00	.00	.00
5	.00	.00	.58	.00	96.79	.00	.58	.00	.00	.00	.00	.00	.00	2.04	.00	.00
6	.00	.00	.00	.00	.00	100.00	.00	.00	.00	.00	.00	.00	.00	.00	.00	.00
7	.00	.00	.00	.00	1.68	.00	98.04	.00	.00	.00	.00	.00	.00	.00	.00	.28
8	.00	.00	5.38	.00	.00	.00	.00	84.95	.00	.00	.00	.00	2.15	.00	7.53	.00
9	.00	.00	.00	.00	.00	.00	.00	.00	97.07	.28	.00	1.54	.98	.00	.14	.00
10	.00	.00	.00	.00	.00	.00	.00	.00	.07	98.36	1.00	.00	.00	.00	.57	.00
11	.00	.00	.00	.08	.00	.00	.00	.00	.16	.00	.90	97.23	.00	.00	1.63	.00
12	.00	.63	.00	.00	.00	.00	.00	.00	.00	1.88	.00	.00	95.63	1.88	.00	.00
13	.00	.00	1.04	.00	.00	.00	.00	.00	1.04	3.11	.00	.00	.00	92.23	.00	2.59
14	.00	.00	4.88	.00	3.66	.00	.00	.00	.00	.00	.00	.00	.00	2.44	89.02	.00
15	.00	.00	.00	.00	.00	.00	.00	.00	.89	.00	2.92	.00	.00	.51	.00	95.69
16	.00	.00	.00	.00	.00	.00	.76	.00	.00	.00	.00	.00	.00	.00	.00	99.24

Over-all Correct Classification = **96.98 %**

1-agricultural, 2-wetland, 3-agricultural, 4-wetland, 5-agricultural, 6-water, 7-agricultural, 8-wetland, 9-bare soil, roads, 10-plains, 11-sand sheets, 12-bare soil, roads, 13-wetland, 14-agricultural, 15-sand dunes, 16-agricultural.

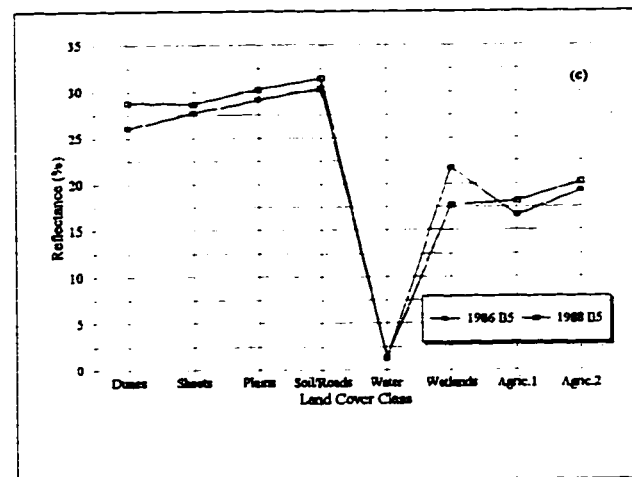
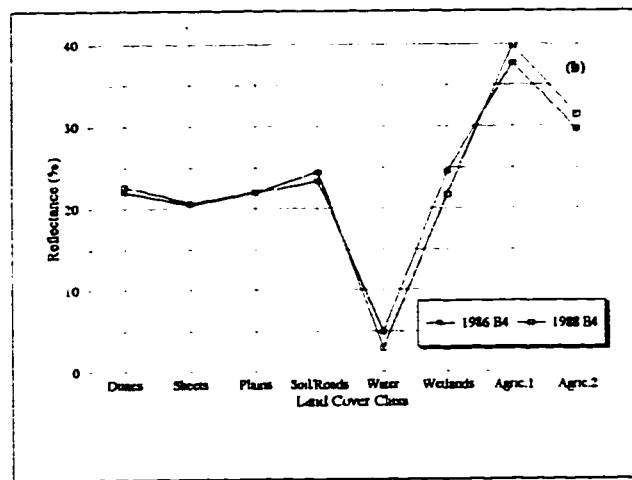
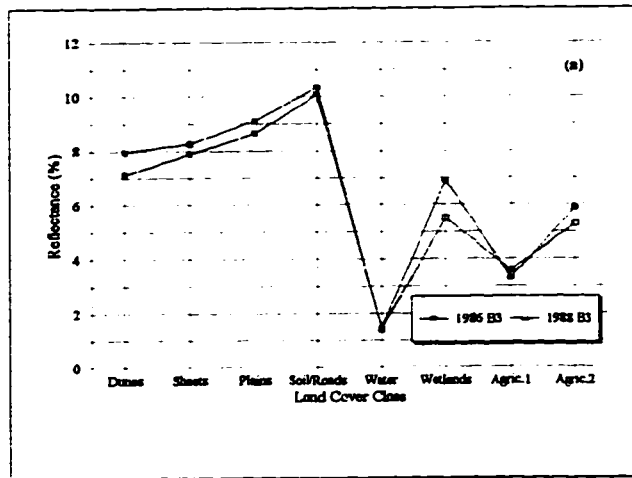


Figure 5-5. Comparison of reflectance curves for eight spectral classes for (a) band 3, (b) band 4, and (c) band 5.



Figure 5-6. Dune change classes for the Rolling Hills dune field. Blue areas correspond to those deposits which were common to both 1986 and 1988. Red areas correspond with deposits which appeared only in the 1986 imagery and purple areas correspond with deposits which appeared only in the 1988 imagery. Scale of the image is 1:200 000.

To account for the areal differences in the two maps, it is helpful to examine the confusion matrices generated from the training statistics. Confusion between clusters results when there is spectral overlap occurring between features. This can be due to different features having similar reflectance values in all spectral bands used in the analysis, such as the similarities that exist between the irrigated crops. Spectral confusion may also relate to boundary pixels, or those pixels associated with zones of transition between adjacent cover types. In natural areas, firm boundaries between cover types rarely exist, rather there is a gradual transition from one cover type to the next. For these boundary pixels, it would be more appropriate to leave them unclassified, but K-means cluster analysis is a forced classifier; that is, every pixel in the scene must be classified. Some pixels are inevitably incorrectly classed. The confusion matrices (Table 5-2 and 5-3) indicate where spectral confusion exists. Table 5-2 shows the confusion matrix for the 1986 training statistics. Overall accuracy was high, 97.26 per cent of the 6240 pixels included in the analysis were correctly classified. Within agricultural regions, confusion occurs almost exclusively between other agricultural classes. For non-agricultural classes, a small amount of confusion exists between the sand dunes, sheets, plains, and soil classes. Confusion also exists between the dunes and wetland class. Similar patterns were observed in the 1988 matrix (Table 5-3), but overall accuracy was slightly lower at 96.98 per cent, and the level of confusion between the sand dunes and wetlands was slightly higher. This confusion is due to the effect of boundary pixels.

Differences between the two years are also evident in the average reflectance curves for the land cover classes, shown in Figure 5-5. Figure 5-5 (a) shows differences in reflectance in band 3 (0.63-0.69 μm). Generally, reflectance is low for all classes, with water and agricultural areas having the lowest values. Reflectance progressively increases for dune, sand sheet, plains, and soil categories. A similar pattern is seen for the 1988 curve, but the values are slightly higher. This would be an expected response if the vegetation is in a state of declined health due to moisture deficits in 1988. Figure 5-5 (b) is a comparison of reflectance curves for band 4 (0.76-0.90 μm). Values are higher for all categories except water. There is little difference between the two years. In 5-5 (c),

curves for band 5 (1.55-1.75 μm) shows lower reflectance in the agricultural classes, with higher reflectance values in the non-agricultural areas. Of these categories, reflectance in the dunes is slightly lower than for the other deposits. Excluding the wetland class, reflectance values are higher for all categories in 1988, suggesting lower plant moisture levels in 1988. These reflectance curves suggest that there are slight differences in vegetative response to moisture deficits between the two years, for the different land cover features. The lower levels of reflectance in bands 3 and 5, and the higher values in band 4, suggest that the vegetation in 1986 is in a healthier state than its counterpart in 1988. It is important to note that there were differences between the two years in the time lapse since the last precipitation event which could account for some of the variation seen. In 1986 Brooks received approximately 23 mm of precipitation five days prior to the acquisition of the imagery and smaller amounts the day before image acquisition. If there was a precipitation event within the bounds of the study area, the vegetation may have 'greened' up prior to image acquisition, and would lead to misleading conclusions.

Examining Figure 5-6 provides further insight as to some of the differences seen in the extent of the dunes between the two years. This image shows areas which were common to both sets of imagery, and areas which were exclusive to either year. The parabolic dunes in the far south eastern part of the dune field appeared only in the 1986 imagery; they were classified as grasslands in the 1988 analysis. In the central part of the scene extensive areas appear as dune deposits in 1988 which are not seen in the 1986 imagery. These are low dunes, being far from the sand source area. They may therefore not retain moisture for as long a time as the thicker deposits and are the first to show the effects of adverse conditions. As a consequence of this inability to retain moisture there will be subtle variations in vegetation on shallower dune deposits. Variations in vegetative vigor, drought resistance, or slight shifts in the proportions of the dominant species will in turn influence the spectral response measured by the satellite.

Although the aeolian and non-aeolian deposits situated in the non-irrigated areas are easily identified on the satellite imagery, it is interesting that different deposits are detected between the wet and dry years. This suggests that there are complex interactions

between the surficial deposits, moisture conditions and the vegetative cover which would be difficult to identify using single date imagery alone. Results of this study reveal that multi-temporal image data is essential for interpretation and mapping of aeolian deposits in southern Alberta. However, without a rigorous assessment of the accuracy of the classified images, it is impossible to state how reliable these images would be for land use mapping purposes. Multi-temporal imagery would also be a useful tool for monitoring change in the region, but once again, correcting the data is especially important in multi-temporal analysis, and comparing the imagery to some type of reference data (maps, air photos, field data, lab spectra, etc.) is needed to establish accurate base information. The results of this study also demonstrates the usefulness of using Landsat TM imagery for stratifying a region into a broad spectrum of land cover types, and using these classes as a guide for planning a more detailed assessment.

Conclusion

Post-classification of imagery for 1986 and 1988 shows that spectral differences exist between the two image dates. Reflectance curves suggest that these slight differences in reflectance show simple vegetative response to moisture differences between 1986 and 1988. If this is the case, the implications for land cover mapping and interpretation of similar regions are that slight differences in moisture can lead to a great deal of variation in the classification results. Multi-temporal data would be valuable in cumulating the area of aeolian deposits accurately. Supplementing this data with auxiliary data such as spectrometer measurements, vegetation surveys, etc. would lead to a deeper understanding as to the field parameters which control the spectral response seen by the satellite.

CHAPTER 6

MULTI-TEMPORAL PRINCIPAL COMPONENT ANALYSIS

Introduction

Principle components analysis (PCA) is a technique frequently used in remote sensing analysis as a means of reducing the redundancy in the information content between bands of satellite imagery, or to reduce the dimensionality of the data set (Lark 1995; Lillesand and Kiefer 1994; Drury 1993). Additionally, it has been used successfully for monitoring and detecting change (Bryne et al. 1980; Richards 1984; 1986; Ingebritsen and Lyon 1985; Fung and LeDrew 1987; Franklin 1991). This chapter examines the principles of PCA, its application to multi-temporal data sets in change detection studies, its use in this study, and the results obtained.

Principal Components Analysis

Principal components analysis (PCA) is frequently used as a means of eliminating some of the redundancy in information content between image bands. This redundancy is due to the high degree of interband correlation that exists in multispectral imagery, meaning that little new information is gained between adjacent image bands (Richards 1986; Fung and LeDrew 1987; Drury 1993; Lillesand and Kiefer 1994). PCA creates new components which are uncorrelated, linear combinations of the original data. The transformation, on a two dimensional data set, is illustrated in Figure 6-1. Figure 6-1 (a) shows the bivariate plot of two bands of data. Due to the high degree of correlation between the bands, the data produces an elongate ellipse of points. PCA shifts the origin

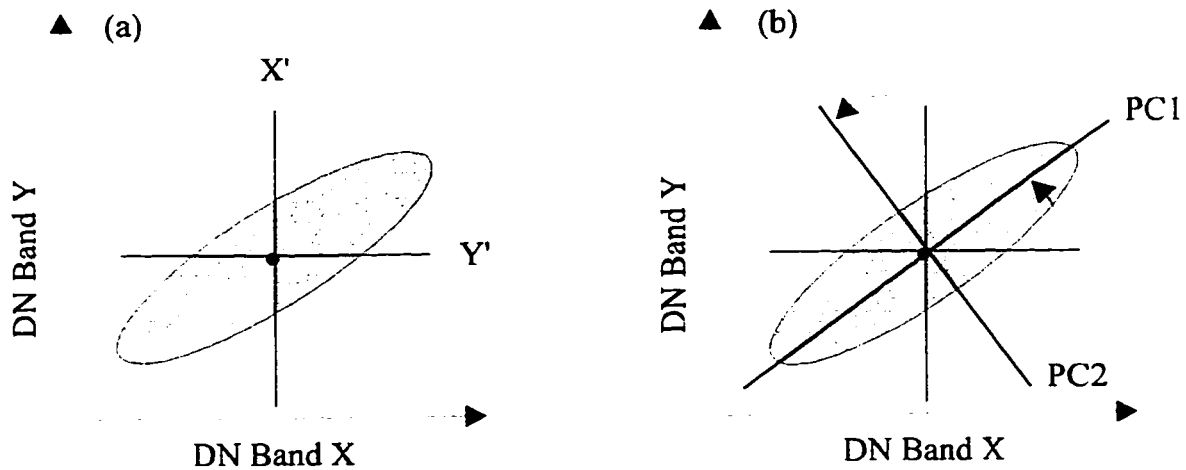


Figure 6-1. The principle component transformation; (a) bivariate plot of correlated data, with axes shifted to mean of the data set, (b) axes are rotated so that PC1 is oriented along the major axis of the ellipse. PC2 is orthogonal to PC1. From Drury (1993).

which represents the mean of the two data sets. In Figure 6-5 (b), the axes are now rotated so that one axis is orientated along the major axis of the ellipse. This is the first principal component along which the data have the greatest degree of spread or variance. The second axis is orthogonal to the first and accounts for the variance not explained by the first principal component. The data points are then projected onto these shifted axes by calculating the covariance matrix for the data set and finding the eigenvectors. The eigenvectors are the coefficients used in the linear equations and determine the contribution of each band to a component. The value for each pixel in the new component is found simply by multiplying the DN in each band by its eigenvector and summing the results (Drury 1993).

These new components are ranked so that the first principle component accounts for the greatest percentage of variance within a scene while higher components account for successively less of the percentage of total variance (Davis 1986; Richards 1986; Fung and LeDrew 1987; Drury 1993; Lillesand and Kiefer 1994). The higher order components are often then excluded from further analysis since they account for little of the scene variance, whereas the greatest amount of information is contained in the first components. This reduces the dimensionality of the data, e.g. from 7 Landsat TM bands to 3, and the components are no longer correlated. However in some cases, relevant information is contained in the higher order components and it would be inadvisable to discard them (Lark 1995). Information contained within the higher order components is the basis of using PCA in change detection studies.

The decorrelation produced by principal component analysis has been shown to be of value in highlighting regions of localized change in multi-temporal Landsat image data (Byrne et al. 1980; Richards 1984; Ingebritsen and Lyon 1985; Fung and LeDrew 1987; Franklin 1991; Ribed and Lopez 1995). This is due to the high correlation that exists between areas of constant cover type and the low degree of correlation that exists between areas of change between image dates (Byrne et al. 1980; Richards 1984; Ingebritsen and Lyon 1985; Ribed and Lopez 1995). Areas associated with constant cover will account for the greatest amount of total scene variance while areas of change will be associated

with only a small portion of the total variance. When all bands of imagery from the years in question are combined into a single data set and analyzed, areas that do not change significantly between image dates will be highly correlated, will account for the greatest proportion of variance in the data set, and will be mapped to the first components. Areas of localized change will show little correlation, will contribute only a small proportion of the overall variance, and will appear in the higher order components. It is then possible to generate change classes by applying classification procedures to the higher order components (Richards 1984; Franklin 1991; Ribed and Lopez 1995).

In this analysis, all bands were merged into a single data set. Standardized PCA was performed using the correlation matrix to calculate the eigenvectors. This resulted in six eigen images. The frequency histograms for each of the resulting eigen images were examined to determine appropriate stretch parameters for enhancing the images for display. Eigen images 1, 2 and 3 accounted for 95 per cent of the total variance in the scene and were used to generate a multi-temporal colour composite.

An alternative approach to change detection is selective PCA (Dwivendi et al. 1993; Chavez and Mckinnon 1994). In this approach, each bandwidth for the period of interest is analyzed as a separate data set. Information that is common to that band in both dates appears in the first component while any change appears in the second component. Using only two images in the transformation greatly simplifies the interpretation of the eigen images, and the nature of the changes which have occurred. It is also possible to create change classes through cluster analysis and classification of the higher order components (Richards 1984). Selective PCA was performed on bands 3, bands 4 and bands 5. The eigen images were examined, and although the second component for band 5 explained only 5.69 per cent of the total variance, it showed areas of change the most clearly. The second component from analysis of band 5 was then classified using the same procedure as previously discussed. The change classes were interpreted using the loading factors and the unclassified eigen image.

Results of Multi-temporal Principal Components Analysis

The six eigen images resulting from PCA of the combined multi-temporal data set are presented in Figure 6-2. Each image was interpreted using the eigenvector loadings for each component as listed in Table 6-1. Of the six components, 95 per cent of the total variance in the data set (see Table 6-1) was contained in components 1, 2 and 3, and these were used to generate the colour composite shown in Figure 6-3. Of the six eigen images produced using selective principle component analysis, each of the second PCs emphasized changes which had occurred between the wet and dry year (see Table 6-2). Band 5 in particular, however, seemed to effectively show differences in moisture between the two years and was selected for classification, using unsupervised methods. The second principle component for band 5 is shown in Figure 6-4 and the resulting class map in Figure 6-5.

Image Interpretation and Discussion

The resulting eigen images are linear combinations of the original bands and can be difficult to interpret based on colour assignment alone. Often the loading factors themselves must be analyzed in order to interpret the eigen images. Examination of the loadings for PC1 (Table 5-1) shows that this component has high positive loadings in bands 3 and 5 for both 1986 and 1988, and high negative loadings in band 4 for both years. This component is a negative measure of overall greenness for the two years, where areas of high amounts of biomass appear dark and areas of lower biomass appear bright. This is seen in Figure 5-2 (a). The second component (b) is an average measure of overall brightness between the 1986 and 1988 imagery, with positive loadings occurring for all bands, particularly in the infrared bands. In PC3 (c) the loadings for 1986 show negative values in bands 3 and 5 and a positive values in band 4. Loadings for the 1988 bands show the reverse pattern, positive loadings in bands 3 and 5 with negative loadings in band 4. This component emphasizes changes in greenness that occurred between the

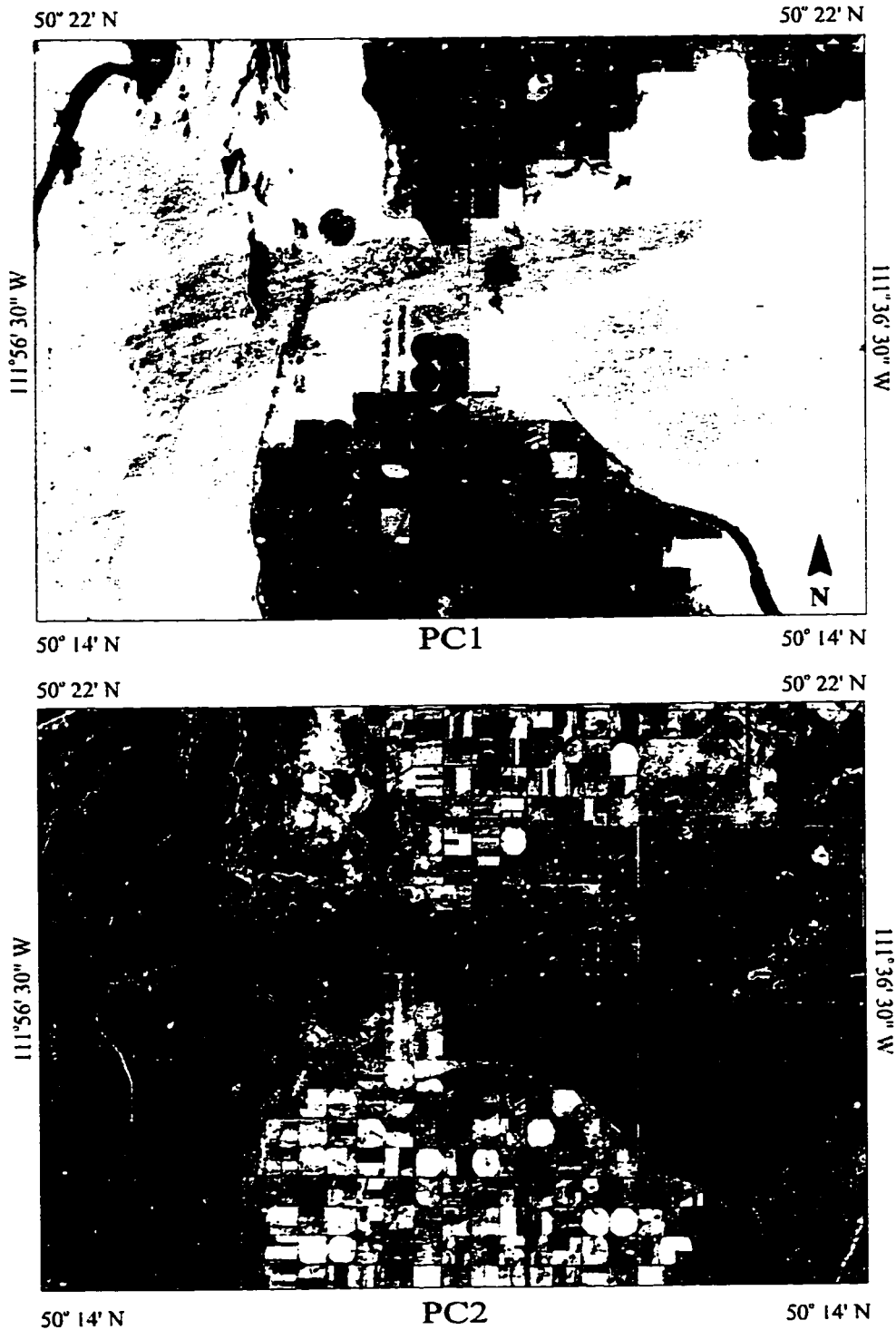


Figure 6-2(a). Eigen images for PCs 1 and 2 for the 1986 and 1988 merged data set. PC1 is a measure of greenness, where features with high biomass appear dark, and areas of low biomass appear bright. PC2 shows overall brightness. Scale of images is 1:200 000.

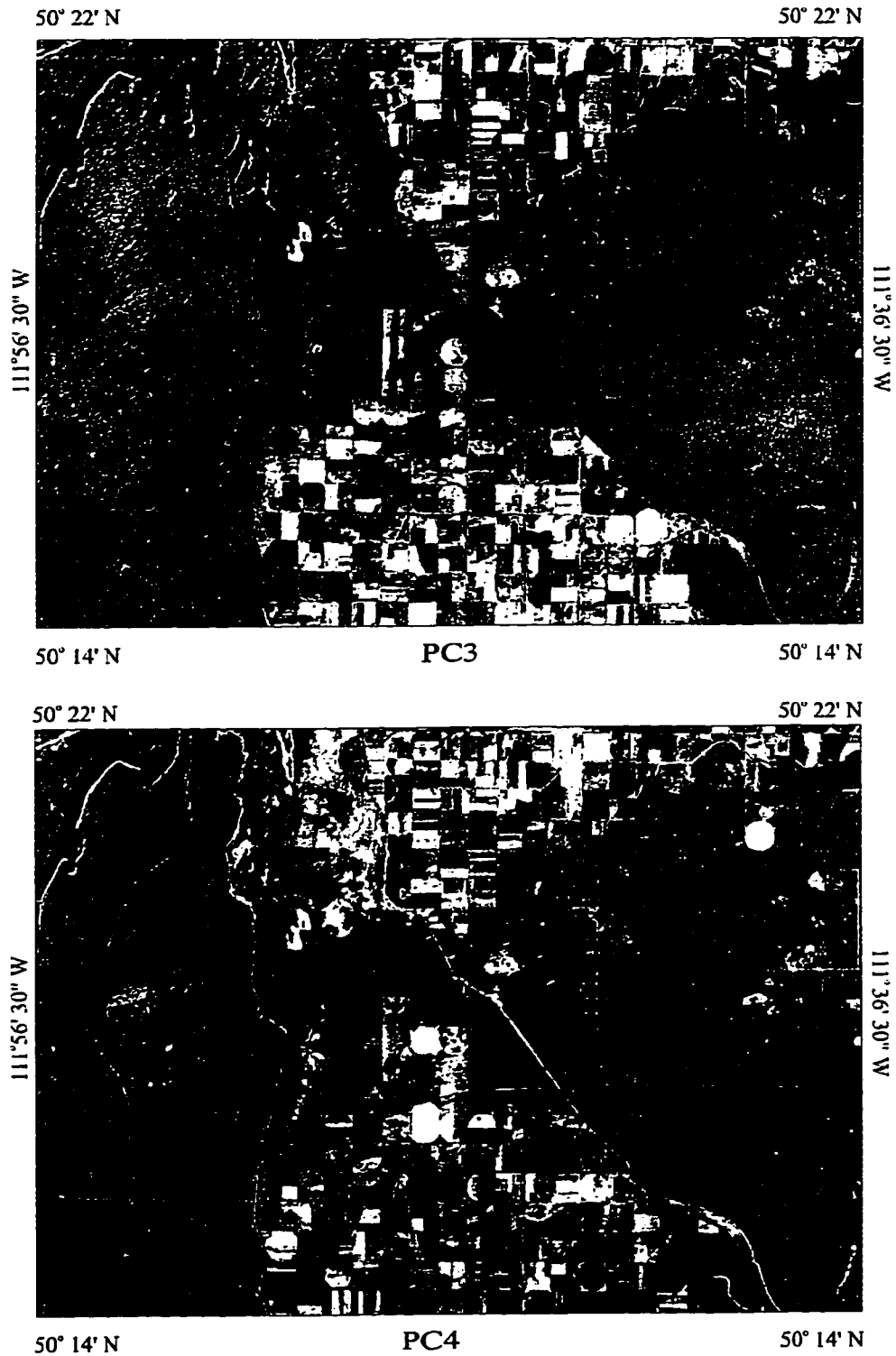


Figure 6-2(b). Eigen images for PCs 3 and 4. PC3 shows decreases in greenness due to differences between the wet and dry year. PC4 shows changes in brightness between the two years. Scale of images is 1:200 000.

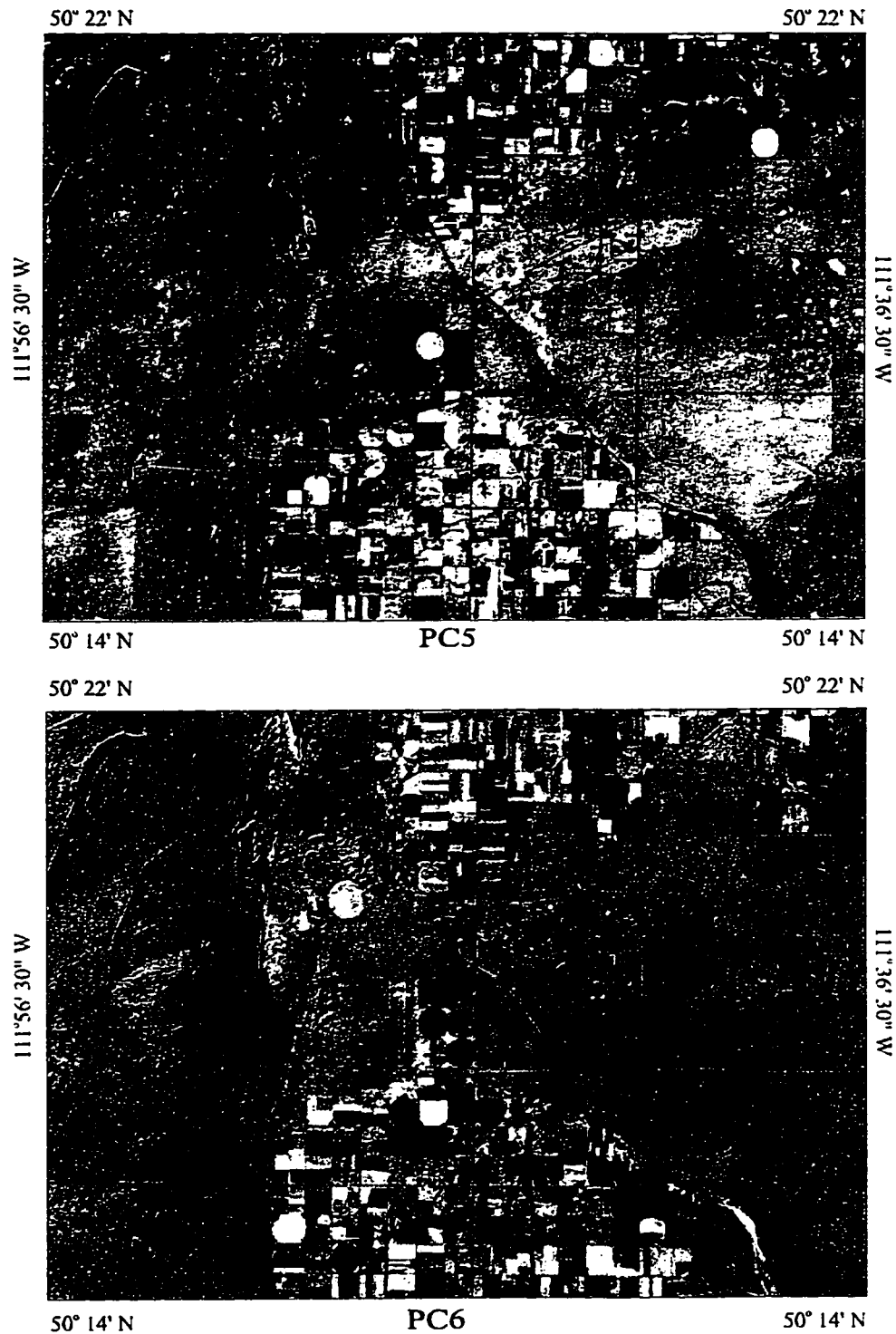


Figure 6-2(c). Eigen images for PCs 5 and 6. PC5 is related to differences in moisture between the wet and dry year. PC6 shows mostly noise. Scale of images is 1:200 000.

Table 6-1. Eigen Structure for Multi-temporal Principle Component Analysis

Band	PC1	PC2	PC3	PC4	PC5	PC6
TM3-86	0.928582	0.160950	-0.267650	0.040663	0.176240	-0.086560
TM4-86	-0.700186	0.649320	0.201241	-0.162514	-0.143620	-0.024137
TM5-86	0.886145	0.363985	-0.180005	-0.193183	0.052367	0.098930
TM3-88	0.925044	0.125512	0.269711	0.190336	-0.119702	0.072368
TM4-88	-0.704733	0.640644	-0.190880	0.225434	0.071758	0.022916
TM5-88	0.889060	0.357709	0.185518	0.002745	0.200197	-0.084339
eigenvalue	4.28	1.13	0.29	0.15	0.11	0.03
%variance	71.34	18.90	4.80	2.54	1.90	0.51
Cumul%	71.34	90.24	95.04	97.58	99.48	99.99

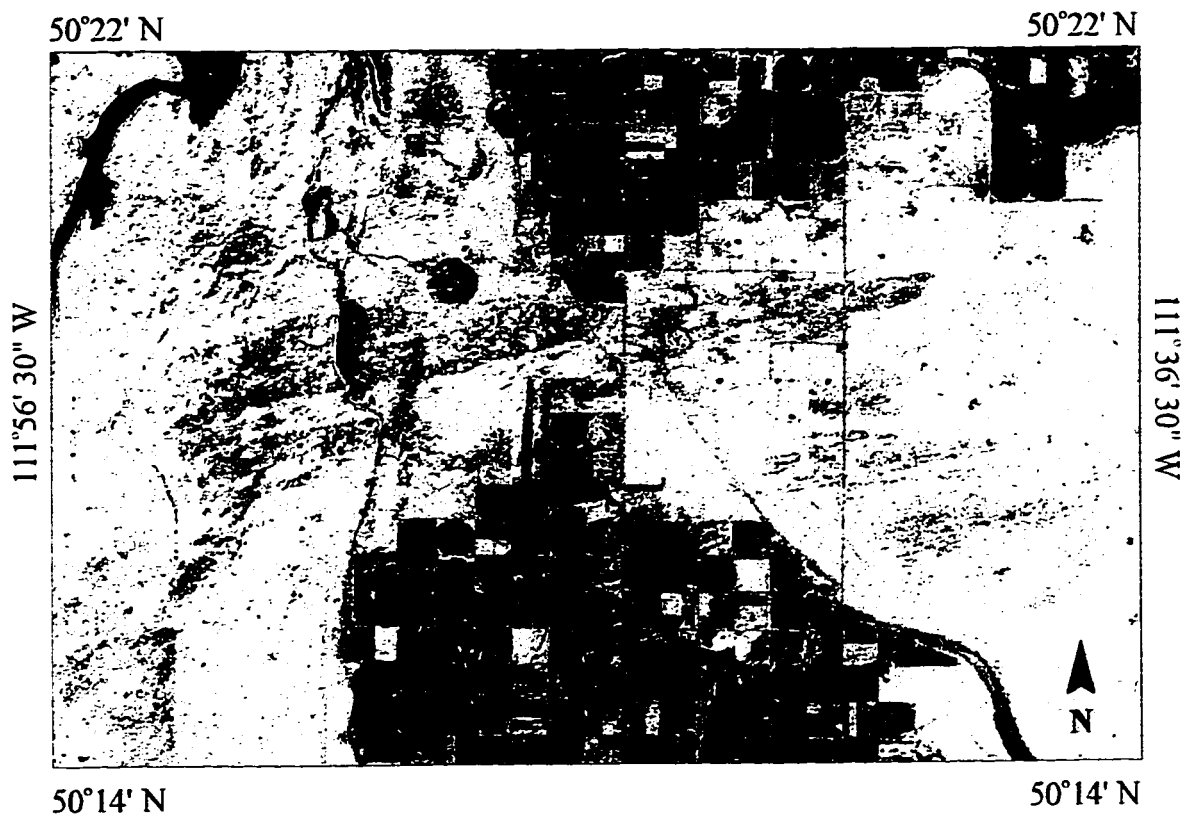


Figure 6-3. Principle component colour composite. PC3 was assigned assigned to blue, PC1 was assigned to green, and PC2 was assigned to red. Scale of image is 1: 200 000.

Table 6-2. Eigen Structure for Selective Principle Component Analysis

	Band	PC1	PC2
(a)	1986-TM3	0.956441	-0.291925
	1988-TM3	0.956441	0.291925
	Eigenvalues	1.83	0.17
	% Variance	91.48	8.52
(b)	1986-TM4	0.954861	-0.297052
	1988-TM4	0.954861	0.297052
	Eigenvalues	1.82	0.18
	% Variance	91.18	8.82
(c)	1986-TM5	0.971148	-0.238477
	1988-TM5	0.971148	0.238477
	Eigenvalues	1.89	0.11
	% Variance	94.31	5.69

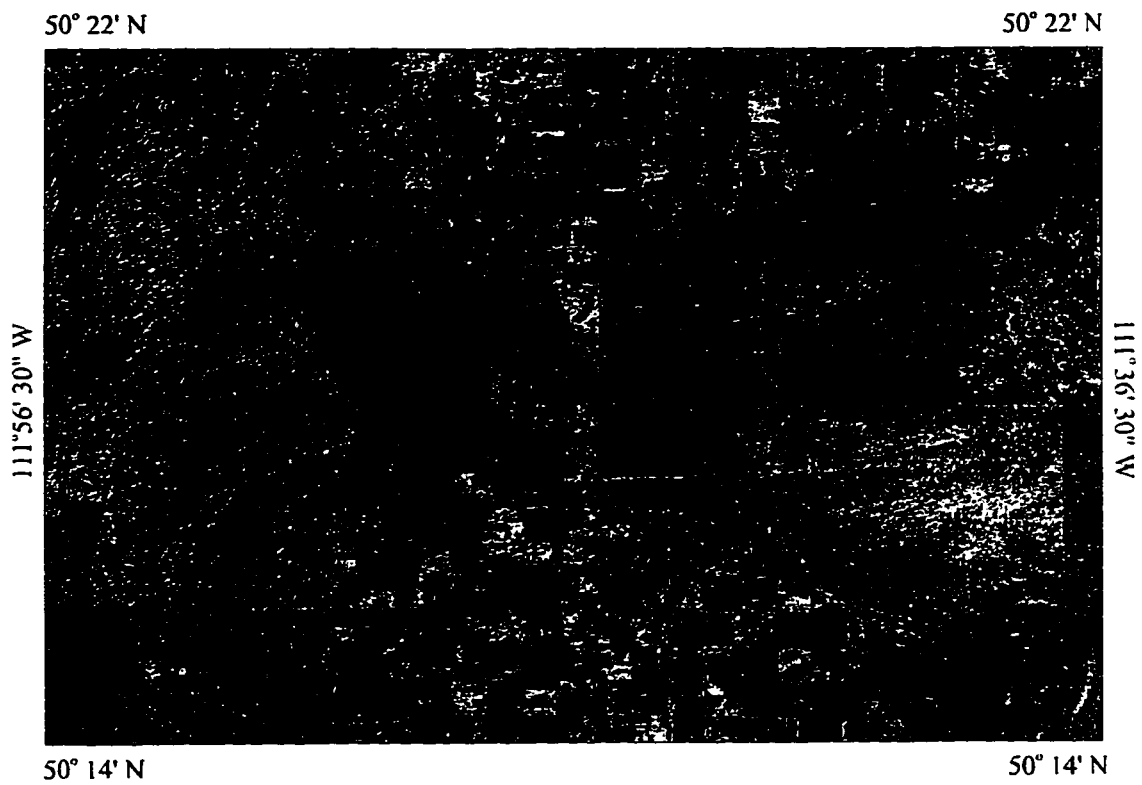
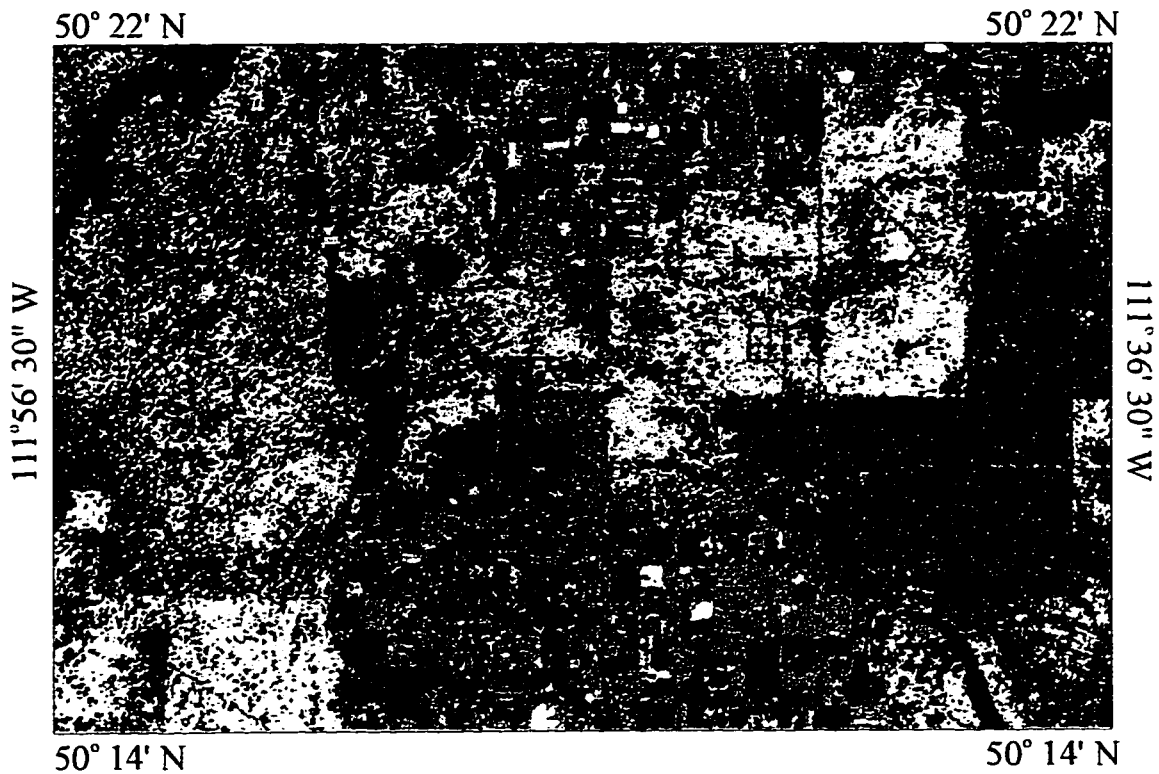


Figure 6-4. PC2 from selective principle component analysis of band 5 for 1986 and 1988. Scale of image is 1: 200 000.










- | | | | |
|---|--|---|---|
|  | Agricultural areas/wetlands/
dunes - areas with higher
moisture in 1986. |  | Agricultural - areas with higher
moisture in 1986. |
|  | Plains areas - less moisture in
1988. |  | Agricultural - areas with higher
moisture in 1986 |
|  | Dune areas/ agricultural -
areas with less moisture in
1988. |  | Agricultural - areas with lower
moisture in 1988. |
|  | Sand sheets/ interdune areas -
areas with higher moisture in
1986. | | Scale: 1: 200 000 |

Figure 6-5. Temporal change classes created from an unsupervised classification of PC 2 of band 5 for 1986 and 1988.

two years. PC 4 (d) is a measure of changes in brightness between the two dates, with 1986 showing negative loadings for the infrared bands and a positive loading in band 3. Loading for 1988 in this component are all positive. Features with increased in brightness are bright in this image whereas features which decreased in brightness appear dark. PC 5 has negative loadings in the visible bands for both years and the near infrared in 1986. The remaining loadings are all positive with the highest value associated with the mid-infrared in 1988. This PC may be related to moisture differences between the two years, where bright features represent areas where there has been a decrease in moisture availability. Finally PC 6 is associated mainly with noise and accounts for less than 1 per cent of the total scene variance. Components 1, 2 and 3 explained the greatest proportion of the total variance in the scene, and were used to create the multi-temporal colour composite (Figure 5-3). The image clearly shows the main dune fields, and larger parabolic dunes are evident in the eastern portion of the scene. The results are similar to those obtained for the unsupervised classification of the 1986 imagery (Figure 5-3) in Chapter 4. Composites generated using the higher order PCs did not yield good results and are not included here.

Interpreting the results obtained from selective PCA was simplified because only two bands were involved in each transformation. In all three bands, loadings for the first component were identical and positive, whereas in PC2, the loading for 1986 was always negative, and for 1988 the loadings were positive (Table 6-2). The second components accounted for little of the overall variance but each contained relevant information regarding change that occurred between the wet and dry year. The second component in band 5 seems to best highlight changes between the two years which were related to differences in moisture. Analysis of the eigen structure for band 5 shows that 94 per cent of the scene variance is recorded in the first component, while 5.69 per cent of total variance appears in PC2 (Figure 6-4). Increases in plant moisture are associated with a decrease in reflectance in band 5 reflectance, so those features which appear darker in this component are associated with higher water content. This included the sand sheet area and the eastern portion of the dune field, while dunes in the southeastern part of the scene appeared very bright.

The basic premise for this work has been that dune forms could be identified on satellite imagery primarily based on vegetative differences which result from soil moisture variations between the different deposits. PC 2 for band 5 suggests that moisture differences exist between the image dates, and the classification of this PC produces temporal classes related to moisture differences. Most noteworthy are the parabolic dunes in the eastern portion of the dune field, which were not visible in the classification of the 1988 imagery (Figure 5-4). In Figure 6-5 these dunes are associated with increases in brightness in band 5 due to a decrease in moisture content during 1988. In contrast, dunes in the western part of the field, nearer the sand source area, appear dark and are associated with higher levels of moisture. Sand sheets in this classification also appear darker, suggesting lower band 5 reflectance in 1986 due to higher water levels.

Conclusion

PCA analysis is as useful technique in analyzing multi-temporal data sets; the transformation can be used to reduce the dimensionality of the data so that fewer bands are used to display the greatest information in the scene, and the new linear components present the information in a way that emphasizes temporal differences in the data set. The rotation of the data may also serve to separate clusters where spectral confusion existed, and result in less confusion in the data when using classification procedures. The selective PCA is useful in that it highlights changes occurring in one band, which simplifies the interpretation of the changes that have occurred. Potential future research could involve a comparison between the performance of PCA and multi-temporal classification procedures for accurately detecting land cover types and detecting changes that occur over time.

CHAPTER 7

CONCLUSION

Introduction

Large areas of semiarid southern Alberta are covered with aeolian sand deposits. At present time the detailed pattern of dune distribution, and their phases of stability and reactivation are not well known. Knowledge of these facts would not only improve our understanding of paleoclimatical and paleoenvironmental conditions but could assist in an assessment of the possible effects climate change. With recent concerns about global warming, understanding the effects of climate fluctuations in the past may be useful in assessing the impact of future climate change (Madole, 1994).

Sand dunes in particular have received a great deal of attention in the literature due to their sensitivity as indicators of past and present change. Understanding the distribution and nature of these deposits is essential for interpreting the landscape, and for understanding change due to fluctuations in climate variables. Past efforts to map these deposits have suffered from a lack of primary data (Mulira, 1986), or because they were left unmapped because of their small size and lack of significant forms (David, 1979). Remotely sensed data, such as that from the Landsat TM, has the potential to alleviate some these problems. This research sought to examine the potential of using Landsat TM data for delineating aeolian deposits in the Rolling Hills area of southern Alberta. Techniques which proved to be effective could then be applied to other areas. Additionally, this study sought to examine the potential of using satellite imagery to detect changes in the deposits due to differences in precipitation between a wet and dry year.

Findings of this Research

Two multi-temporal image processing techniques were examined for their ability to differentiate aeolian from non-aeolian deposits, and to differentiate change that had occurred between the two years due to moisture differences. The first, post-classification comparison of the two image sets compared the data after each has been classified independently. The results suggested that both image sets, from the wet or dry year, were able to delineate the features of interest but with extensive differences between classification results. The implication is that for land cover class mapping, using satellite imagery to classify the data based on its spectral characteristics may be an effective way of stratifying the area into broad classes which can be used to direct more extensive field mapping. Without assessing the accuracy of the classification, however, it is uncertain how representative these spectral classes are of ground conditions. In conjunction with this problem, spectral characteristics of features, as measured by satellite, can be highly variable due to atmospheric effects. These affects need to be normalized so that image to image comparisons can be made. The implication for detecting and monitoring change is that a known accurate reference is required before a measurement of real change can be made. Comparison of the spectral characteristics for the two image dates provides a qualitative measure of spectral change between those dates, but when nothing is known of how accurately the classification represents conditions in the field, the extent of true change between the features can not be known with any certainty.

The second technique, principle component analysis using the merged multi-temporal data set was also effective at delimiting the various land cover components. The results showed that information common to both scenes appeared in the first few components, where as areas highlighting change were seen in higher order components. Selective principle components analysis showed that band 5 in particular emphasized relative moisture differences between the two years. To quantify these differences, field measurements of soil moisture would be needed.

Conclusion

In summary, the main finding of this work is that satellite images have the potential to be a valuable tool in mapping these deposits, and in change detection and monitoring applications. However, this data needs to be supplemented with ground data, preferably collected at the time of image acquisition, in order to calibrate the satellite data to ground spectral measurements, and as ground reference data with which the satellite imagery can be compared. This will give a fuller and more accurate assessment of the satellite's ability to accurately discriminate represent ground conditions and provide a better basis for interpretation.

WORKS CITED

- Blount, G., Smith, M. O., Adams, J. B., Greeley, R., and Christensen, P. R. 1990. Regional aeolian dynamics and sand mixing in the Gran Desierto: Evidence from Landsat Thematic Mapper images *Journal of Geophysical Research*, 95 (B10): 15463-15482.
- Bryan, R. B., Campbell, I. A., Yair, A. 1987. Postglacial geomorphic development of the Dinosaur Provincial Park badlands, Alberta. *Canadian Journal of Earth Science*, 24: 135-146.
- Breed, C. S., Fryberger, S. G., Andrews, S., McCauley, C., Lennartz, F., Gebel, D. and Horstman, K. 1979. Regional studies of sand seas, using Landsat (ERTS) imagery, *in A Study of Global Sand Seas* (E. D. McKee, editor), USGS Prof. Paper 1052, pp305-397.
- Breed, C. S. and Grow, T. 1979. Morphology and distribution of dunes in sand seas observed by remote sensing, *in A Study of Global Sand Seas* (E. D. McKee, editor), USGS Prof. Paper 1052, pp. 253-302.
- Byrne, G. F., Crapper, P. F., and Mayo, K. K. 1980. Monitoring land-cover change by principle component analysis of multitemporal Landsat data. *Remote Sensing of Environment*, 10: 175-184.
- Chavez, P. S. 1989. Radiometric calibration of Landsat Thematic mapper multispectral images. *Photogrammetric Engineering and Remote Sensing*, 55: 1285-1294.
- Chavez, P. S., and MacKinnon, D. J. 1994. Automatic detection of vegetation changes in the southwestern United States using remotely sensed images. *Photogrammetric Engineering and Remote Sensing*, 60: 571-583.
- Christiansen, E. A. 1979. The Wisconsinan deglaciation of southern Saskatchewan and adjacent areas. *Canadian Journal of Earth Sciences*, 16: 913-938.
- Clayton, L. and Moran, S. R. 1982. Chronology of Late Wisconsinan Glaciation in Middle North America. *Quaternary Science Reviews*, 1: 55-82.

- Coupland, R. T. 1950. The ecology of mixed prairie in Canada. *Ecological Monographs*, 20: 271-315.
- _____, 1952. Grassland communities of the western Canadian prairies-climax and subclimax, in *Proceedings of the 6th International Grasslands Congress*, pp. 625-631.
- _____, 1961. A reconsideration of grassland classification in the Northern Great Plains of North America. *Journal of Ecology*, 49: 135-167.
- David, P. P. 1977. *Sand Dune Occurrences of Canada. A Theme and Resource Inventory Study of Eolian Landforms of Canada*. Indian and Northern Affairs, National Parks Branch Contract No. 74-230, 174 pp.
- _____, 1988. The Coeval Eolian Environment of the Chaplain Sea Episode, in *The Late Quaternary Development of the Champlain Sea Basin* (Gadd, N. R., editor), Geological Association of Canada Special Paper 35, pp. 291-305.
- _____, 1993. Great Sand Hills of Saskatchewan: An Overview in *Quaternary and Late Tertiary Landscapes of Southwestern Saskatchewan and Adjacent Areas* (Sauchyn, D.J., editor). Canadian Plains Research Center, Regina. pp.59-81.
- Davis, J. C. 1986. *Statistics and Data Analysis in Geology*, Second edition. John Wiley and Sons, Toronto, 646 pp.
- Drury, S. A. 1993. *Image Interpretation in Geology*, Second edition. Chapman and Hall, London, 283 pp.
- Dwivedi, R. S., Sankar, T. R., Venkataratnam, L. and Rao, D.P. 1993. Detection and delineation of various desert terrain features using Landsat-TM derived image transforms. *Journal of Arid Environments*, 25:151-162.
- Eastman, J. R. 1995. *IDRISI for Windows, version 1.0*. A Geographical information systems software package, Clark University, Worcester, Massachusetts.
- Elachi, C. 1987. *Introduction to the Physics and Techniques of Remote Sensing*. John Wiley and Sons, New York, 413 pp.
- Environment Canada, 1993. *Canadian Climatic Normals- Prairie Provinces, 1960-1990*. Atmospheric and Environmental Services, Ottawa, CD ROM.

- Evans, D. J. A., and Campbell, I. A. 1992. Glacial and postglacial stratigraphy of Dinosaur Provincial Park and surrounding plains, southern Alberta, Canada. *Quaternary Science Reviews*, 2: 535-555.
- Eyton, J. R. 1992. *TERRA FIRMA*, a cartographic display package, University of Alberta, Edmonton, Alberta.
- Franklin, J. 1991. Land cover stratification using Landsat Thematic Mapper data in Sahelian and Sudanian woodland and wooded grassland. *Journal of Arid Environments*, 20: 141-163.
- Forman, S. L., Goetz, A. F. H., and Yuhas, R. H. 1992. Large-scale stabilized dunes on the High Plains of Colorado: Understanding the landscape response to Holocene climates with the aid of images from space. *Geology*, 20: 145-148.
- Fung, T. and LeDrew, E., 1987. Application of Principal Components Analysis to change detection. *Photogrammetric Engineering and Remote Sensing*, 53:1649-1658.
- Gaylord, D. R. 1982. *Geologic History of the Ferris Dune Field, south - central Wyoming*. Geological Society of America, Special Paper 192. pp. 65-82.
- Gaylord, D. R. 1990. Holocene paleoclimatic fluctuations revealed from dune and interdune strata in Wyoming. *Journal of Arid Environments*, 18: 123-138.
- Gaylord, D. R. and Stetler, L. D., 1994., Aeolian - climatic thresholds and sand dunes at the Hanford Site, south - central Washington, U.S.A. *Journal of Arid Environments*, 28: 95-116.
- Goossens, E. M. C., De Roover, B. P., and Goossens, R. E. A. 1993. A digital approach to the separation of parabolic sand dune areas from interdunal areas using Landsat MSS data. *Journal of Arid Environments*, 25:131-140.
- Gullet, D. W. and Skinner, D.W. 1992. *The State of Canada's Climate: Temperature Change in Canada 1895 - 1991*. A State of the Environment Report, Atmospheric Environment Service, Environment Canada SOE Report No. 92-2, pp. 36.
- Hemenway, D. 1994. *Q-SURF*, a multiquadric surfacing program, Department of Geography, University of Alberta, Edmonton, Alberta.
- Hemenway, D. 1992. *FILTER*, a data point reduction program, Department of Geography, University of Alberta, Edmonton, Alberta.

- Heute, A. R. 1988. A soil- adjusted vegetation index (SAVI). *Remote Sensing of Environment*, 25: 295-309.
- Ingebritsen, S. E. and Lyon, R. J. P. 1985. Principal components analysis of multitemporal image pairs. *International Journal of Remote Sensing*, 6: 687-696.
- Jacobberger, P. A., and Hooper, D. M. 1991. Geomorphology and reflectance patterns of vegetation-covered dunes at the Tsodilo Hills, north-west Botswana. *International Journal of Remote Sensing*, 12: 2321-2342.
- Jensen, J. R. 1986. *Introductory Digital Image Processing*. Prentice Hall, New York, 99-116 pp.
- Jorgensen, D. W. 1992. Use of soils to differentiate dune age and to document spatial variation in eolian activity; northeast Colorado, U.S.A. *Journal of Arid Environments*, 23: 19-34.
- Kaushalya, R. 1992. Monitoring the impact of desertification in western Rajasthan using remote sensing. *Journal of Arid Environments*, 22: 293-304.
- Kerr, D. S., Morrison, L. J., and Wilkinson, K. E. 1993. *Reclamation of Native Grasslands in Alberta: A Review of the Literature*. Alberta land Conservation and Reclamation Council Report No. RRTAC93-1, 205 pp.
- Kimes, D. S. 1991. Radiative transfer in homogeneous and heterogeneous vegetation canopies in *Photon-Vegetation Interactions: Applications in Optical Remote Sensing and Plant Ecology* (Myerini, R. B., and Ross, J., editors). Springer-Verlag, Berlin, pp. 302-334.
- Kjearsgaard, A. A., Peters, T. W., and Pettapeice, W. W. 1983. *Soil Survey of the County of Newell, Alberta*. Alberta Soil Survey Report No. 41, 138 pp.
- Kolm, K. E. 1982. Predicting the surface wind characteristics of southern Wyoming from remote sensing and eolian geomorphology, in *Interpretation of Windflow Characteristics from Eolian Landforms*. (Marrs, R.W. and Kolms, K.E. editors). Geological Society of America Special Paper 192, 109 pp.
- Lark, R. M. 1995. Contributions of principle components to discrimination of classes of land cover in multi-spectral imagery. *International Journal of Remote Sensing*, 16: 779-787.

- Lemmen, D. S. 1996. Geologic Setting, *in Landscapes of the Palliser Triangle: Guidebook for the Canadian Geomorphology Research Group Field Trip* (D. S. Lemmen, editor). Canadian Association of Geographers, Annual Meeting, Saskatoon, 92 pp.
- Lillesand, T. M., and Kiefer, R. W. 1994. *Remote Sensing and Image Interpretation*, Third Edition. John Wiley and Sons, Toronto, 750 pp.
- Lloyd, D. 1990. A phenological classification of terrestrial vegetation cover using shortwave vegetation index imagery. *International Journal of Remote Sensing*, 11: 2269-2279.
- Looman, J. 1983. *111 Range and Forage plants of the Canadian Prairies*. Research Branch, Agriculture Canada Publication 1751, Ottawa., 255 pp.
- Madole, R. F. 1994. Stratigraphic evidence of desertification in the west-central Great Plains within the past 1000 years. *Geology*, 22: 483-486.
- Markham, B. L., and Barker, J. L. 1986. Landsat MSS and TM post-calibration dynamic ranges, exoatmospheric reflectances and at-satellite temperatures, *in Eosat Landsat Technical Notes*, pp. 3-8.
- Marrs, R. W. and Gaylord, D. R. 1982. Techniques for interpretation of windflow characteristics from eolian landforms., *in Interpretation of Windflow Characteristics from Eolian Landforms*. (Marrs, R.W. and Kolms, K.E. editors). Geological Society of America Special Paper 192, 109 pp.
- Mossop, G. and Shetson, I. (Compilers) 1994. *Geological Atlas of the Western Canada Sedimentary Basin*. Calgary, Canadian Society of Petroleum Geologists and Alberta Research Council, 510 pp.
- Muhs, D. R., and Holliday, V. T. 1995. Evidence of active dune sand on the Great plains in the 19th century from the accounts of early explorers. *Quaternary Research*, 43: 198-208.
- Muhs, D. R., and Maat, P. B. 1993. The potential response of eolian sands to green house warming and precipitation reduction on the Great Plains of the U. S. A. *Journal of Arid Environments*, 25:351-361.
- Mulira, J. E. 1986. *Eolian Landforms of Alberta*, Alberta Forestry, Lands and Wildlife, Resource Evaluation and Planning and Public Lands Divisions, Edmonton, Alberta, pp. 50.

- Murphy, L. L. 1996. *Mapping of Aeolian Dune Boundaries in Southern Alberta Using Landsat Thematic Mapper Data for a Wet and a Dry Period*. Unpublished M.Sc. thesis, University of Alberta, Edmonton, Alberta, 71 pp.
- Paisley, C. I., Lancaster, N., Gaddis, L. R., and Greeley, R. 1991. Discrimination of active and inactive sand from remote sensing; Kelso Dunes, Mojave Desert, California. *Remote Sensing of Environment*, 37: 153-166.
- Paterson, J. 1996. *The Development of Glacial Lake Bassano During the Late Pleistocene in Southern Alberta*. Unpublished M.Sc. thesis, University of Alberta, Edmonton, Alberta, 188 pp.
- Porter, M. 1995. *North Rolling Hills Area, Site Plan*. Eastern Irrigation District, Brooks, Alberta, scale 1: 30 000.
- Proudfoot, W. 1994. *Climatic change and Environmental Implications in the Medicine Hat Area Using Billings Montana as an Analogue*. Unpublished M.Sc. thesis, University of Alberta, Edmonton, Alberta, 28 pp.
- Ribed, P. S., and Lopez, A. M. 1995. Monitoring burnt areas by principal components analysis of multi-temporal TM data. *International Journal of Remote Sensing*, 16: 1577-1587.
- Richards, J. A. 1984. Thematic mapping from multitemporal image data using the principle components transformation. *Remote Sensing of Environment*, 16: 35-46.
- _____, 1986. *Remote Sensing Digital Image Analysis. An Introduction*, Springer - Verlag, Berlin, 281 pp.
- Rivard, B. 1997. Personal communication. Department of Earth and Atmospheric Science, University of Alberta.
- Robinove, C. J., Chavez, P. S., Gehring, D., and Holmgren, R. 1981. Arid land monitoring using Landsat albedo difference images. *Remote Sensing of Environment*, 11: 133-156.
- Roesler, A. 1995. *Late Holocene Dune Activity, Rolling Hills Lake Sand Hills, Southeastern Alberta*. Unpublished honors thesis, University of Alberta, Edmonton, Alberta, 65 pp.
- Shetsen, I. 1987. *Quaternary Geology, southern Alberta*. Alberta Research Council, Edmonton, Alberta, scale 1; 500 000.

- Stokes, S., and Gaylord, D. R. 1993. Optical dating of Holocene dune sands in the Ferris dune field, Wyoming. *Quaternary Research*, 39: 274-281.
- Strong, W. L. 1992. *Ecoregions and Ecodistricts of Alberta*, vol 1 & 3. Alberta Forestry, Lands and Wildlife, Land Information Services Division, Resource Information Branch, Edmonton., Alberta, pp. 77 & 259.
- Thomas, D. S. G. 1989. *Arid Zone Geomorphology*. Belhaven Press, London, 372 pp.
- Tueller, P. 1987. Remote sensing science applications in arid environments. *Remote Sensing of Environment*, 23:143-154.
- Vance, R. E., and Wolfe, S. A. 1996. Climate in *Landscapes of the Palliser Triangle: Guidebook for the Canadian Geomorphology Research Group Field Trip* (D. S. Lemmen, editor). Canadian Association of Geographers, Annual Meeting, Saskatoon, 92 pp.
- Vreeken, W. J. 1989. Late Quaternary events in the Lethbridge area, Alberta. *Canadian Journal of Earth Science*, 26: 551-560.
- Vreeken,, W.J., 1993. Postglacial soil-landscape regimens in the Palliser Triangle, in *The Palliser Triangle: A Region in Space and Time* (Barendregt, R.W., Wilson, M.C., and Jankuis, F.J., editors). University of Lethbridge, Lethbridge, pp. 125-152.
- Walter-Shea, E. A., and Norman, J. M. 1991. Leaf optical properties in *Photon-Vegetation Interactions: Applications in Optical Remote Sensing and Plant Ecology* (Myeneri, R. B., and Ross, J., editors). Springer-Verlag, Berlin, pp. 229-250.
- Wolfe, S. A., Huntley, D. J., Ollerhead, J. 1995. Recent and late Holocene sand dune activity in southwestern Saskatchewan in *Current Research 1995-B: Geological Survey of Canada*, pp. 131-140.

APPENDIX I. GEOMETRIC RECTIFICATION

Geometric rectification involves transforming the image geometry so that it is planimetric (Jensen 1986). This involves finding the mathematical relationship that exists between the image pixel locations and the location of the corresponding pixels on a map, and applying the transformation to every pixel in the original image to relocate it to its proper position in the rectified image. This process is referred to as spatial interpolation and involves finding the coordinates of ground control points, which are features which can be positioned on both the original image and on a map, and modeling the geometric distortion present. This generally requires a least squares fit of polynomial equations to the ground control points (Jensen 1986). The expression used is

$$x' = a_0 + a_1x + a_2y$$

$$y' = b_0 + b_1x + b_2y$$

where x and y are positions in the rectified output image and x' and y' are the corresponding positions in the original input image. The six coefficients model distortions in the scene such as translation in x and y , scale changes in the x and y direction, skew, and rotation, without the need to identify the specific source of the distortion (Jensen 1986).

Before rectifying the entire data set, it is necessary to determine how well the six coefficients account for the geometric distortion present in the image. Calculating the root mean square error (RMS_{error}) for each of the ground points gives an indication of the amount of distortion that was not corrected for in the coordinate transformation. The RMS_{error} is calculated using the formula

$$RMS_{error} = \sqrt{(x' - x_{original})^2 + (y' - y_{original})^2}$$

where $x_{original}$ and $y_{original}$ are the original coordinates of the GCP in the image, and x' and y' are the computed or estimated coordinates in the original image. Ideally these values would be identical, indicating that all geometric distortion has been accounted for by the model, but this rarely occurs. Any discrepancies between the values shows the amount of

distortion not accounted for in the transformation. If the level of error for a particular GCP exceeds a user specified threshold, the point is either re-evaluated or omitted from the final calculations. Once an acceptable level of RMS_{error} is reached, the coordinate transformation is applied to the entire image. Table I-1 and Table I-2 list the GCP coordinates used to rectify the Landsat TM scene used in this study and the RMS_{error} associated with each point. Two points were omitted from the final transformation because the amount of error was unacceptably high. Table I-3 lists the coefficients used to rectify the images.

Table I-1. Coordinates of the Ground Control Points Used to Rectify the 1986 Landsat TM Scene

X-original	Y-original	X-rectified	Y-rectified	Residual
184.0	989.0	437300	5583000	1.658612
510.0	891.0	445400	5582900	2.637512
706.0	890.0	450300	5582800	0.708109
954.0	887.0	456550	5582750	2.320110
964.0	771.0	456750	5579800	0.507585
769.0	729.0	451900	5578750	1.101225
573.0	699.0	447000	5578000	1.614176
445.0	763.0	443750	5579650	1.812560
30.0	889.0	433450	5582850	1.311272
443.0	634.0	443750	5576400	1.071477
508.0	633.0	443750	5576400	0.636452
833.0	622.0	445350	5576000	3.981707
507.0	483.0	453500	5572700	2.460080
506.0	373.0	445300	5569900	0.379993
111.0	249.0	435450	5566800	1.502014
505.0	243.0	445300	5566300	omitted
931.5	434.5	455950	5571450	1.703725
768.5	153.0	451850	5564400	0.504165
239.0	92.5	438650	5562950	1.430363
474.5	115.0	446100	5563400	omitted

Overall RMS = 1.759654 meters

Table I-2. Coordinates of the Ground Control Points Used to Rectify the 1988 Landsat TM Scene.

X-original	Y-original	X-rectified	Y-rectified	Residuals
198.5	892.0	437300	5583000	3.520865
525.0	886.0	445400	5582900	0.744416
721.0	883.0	450300	5582800	0.501632
969.0	881.0	456550	5582750	2.119229
980.0	764.0	456750	5579800	1.221372
784.0	721.0	451900	5578750	0.654350
589.0	692.0	447000	5578000	1.676062
458.0	756.0	443750	5579650	0.234846
46.0	878.0	433450	5582850	4.110597
458.0	626.0	443750	5576400	0.242645
523.0	626.0	445350	5576400	0.736250
849.0	615.0	453500	5576000	3.435879
522.0	477.0	445300	5572700	2.059348
520.0	367.0	445300	5569900	0.925591
126.0	242.0	435450	5566800	1.630323
518.0	238.0	445300	5566300	omitted
945.5	428.0	455950	5571450	2.353283
783.0	146.5	451850	5564400	0.853338
253.0	86.0	438650	5562950	1.346011
489.0	108.0	446100	5563400	omitted

Overall RMS = 1.938133 meters

Table I-3. Coefficients Used to Rectify the 1986 and 1988 Landsat TM Scenes

Coefficient	X	Y
1986		
a_0	-17089.73893	-222744.60889
a_1	0.04003	0.00011
a_2	-0.00004	0.04005
1988		
a_0	-17310.88789	-222534.05383
a_1	0.04004	0.00018
a_2	-0.00000	0.04000

APPENDIX II. LANDSAT THEMATIC MAPPER DATA CALIBRATION

Landsat Thematic Mapper data is quantized to byte values (8 bit digital numbers) prior to distribution. However, to facilitate comparison of imagery acquired for different dates, it is necessary to convert the DNs back to spectral radiance. The data is radiometrically calibrated using data obtained from internal calibration targets situated near the detectors and sampled at the end of each scan. The digital numbers are converted to spectral radiance using the following equation (Markham and Barker 1986):

$$I\lambda = L_{\min}\lambda + [(L_{\max}\lambda - L_{\min}\lambda) / DN_{\max}] DN$$

where $I\lambda$ = spectral radiance in $mW\ cm^{-2}\ ster^{-1}\ \mu m^{-1}$

$L_{\min}\lambda$ = spectral radiance at $DN = 0$

$L_{\max}\lambda$ = spectral radiance at $DN = DN_{\max}$

DN = spectral radiance expressed as an 8 bit number

DN_{\max} = maximum DN value after radiometric calibration, 255 for 8 bit data

Postcalibration spectral radiance values for $L_{\min}\lambda$ and $L_{\max}\lambda$ are shown in Table III-1.

Converting spectral radiance to at-satellite reflectance further reduces variability between scenes by normalizing for solar irradiance (Markham and Barker 1986).

Effective at-satellite reflectance is given by (Markham and Barker 1986):

$$\rho_p = (\pi * I\lambda * d^2) / (E_{\text{sun}}\lambda * \cos\theta_s)$$

Where ρ_p = unitless effective at-satellite reflectance, which combines surface and atmospheric reflectance of the Earth

$I\lambda$ = spectral radiance in $mW\ cm^{-2}\ ster^{-1}\ \mu m^{-1}$

d = Earth-Sun distance in astronomical units = (1.014 for August 1)

$E_{\text{sun}}\lambda$ = mean exoatmospheric irradiance in $mW\ cm^{-2}\ \mu m^{-1}$

θ_s = solar zenith angle in degrees

Values for $E_{\text{sun}}\lambda$, for Landsat-5, are listed in Table III-1.

Table II-1. Landsat TM Post-calibration Spectral Radiances and Solar Irradiances

TM band	$L_{\min}\lambda$	$L_{\max}\lambda$	$E_{\text{sun}}\lambda$
1	-0.150	15.210	195.700
2	-0.280	29.680	182.900
3	-0.120	20.430	155.700
4	-0.150	20.620	104.700
5	-0.037	2.719	21.930
7	-0.015	1.438	7.452

Data from Markham and Barker (1986).

APPENDIX III. HILLSHADE MODEL OF THE ROLLING HILLS AREA

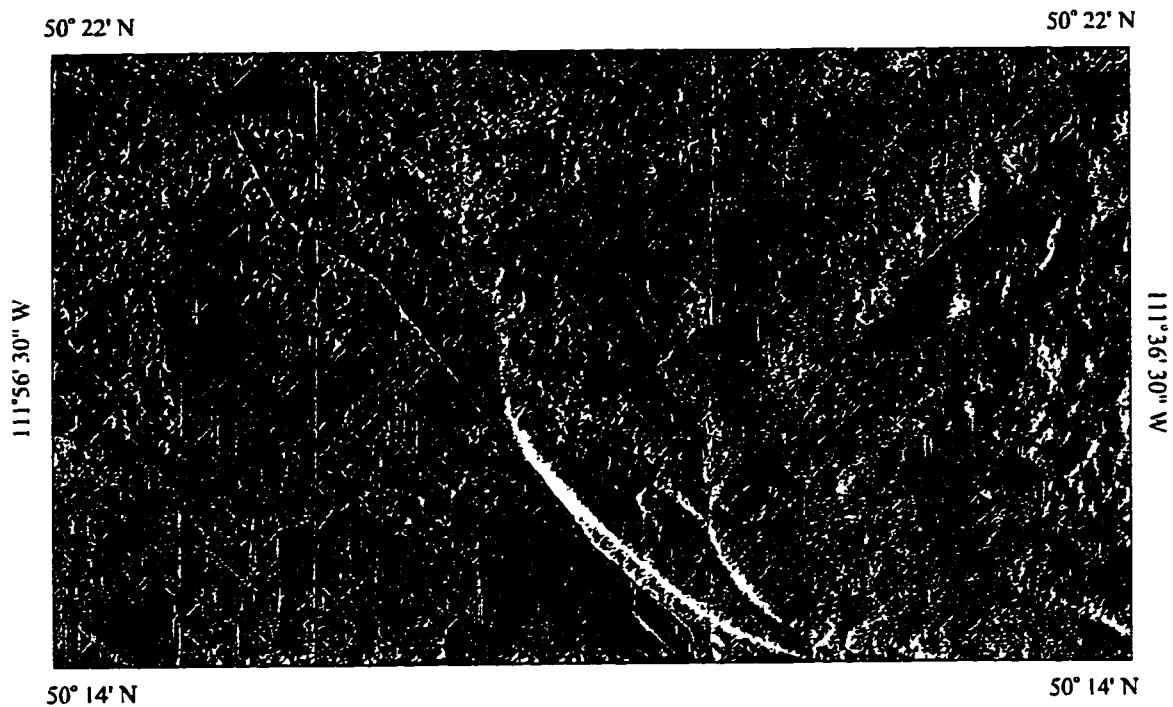


Figure III.1. Hillshade model of the Rolling Hills area in southern Alberta. Area A corresponds to the main dune field. Model was created using a digital elevation model generated from a 1 m contour interval topographic map (Porter 1995). Scale of image is 1:200 000.